# Fission yeast polycystin Pkd2p promotes transition to cell growth during cytokinesis

Debatrayee Sinha[1], Denisa Ivan[1], Ellie Gibbs[2], Madhurya Chetluru[1], John Goss[2] and Qian Chen[1*]

* Correspondence: qian.chen3@utoledo.edu

[1]: Department of Biological Sciences

University of Toledo

2801 West Bancroft ST

Toledo, OH, 43606

[2]: Department of Biological Sciences

Wellesley College

106 Central Street

Wellesley, MA 02482

Running title: Pkd2p antagonizes SIN, Pkd2p promotes interphase cell growth

Abbreviations: Septation initiation network (SIN), Spindle pole bodies (SPBs), Morphogenesis Orb6 related (MOR)

**Abstract**:

Polycystins are evolutionally conserved cation channels. Mutations of human polycystins lead to a common genetic disorder, Autosomal Dominant Polycystic Kidney Disorder. Interestingly, the fission yeast polycystin homologue Pkd2p is required for cytokinesis, the last stage of cell division, but the mechanism remains unclear. Motivated by our discovery of the epistatic genetic interactions between *pkd2* and the Hippo pathway Septation Initiation Network (SIN), we investigated their interplay during cytokinesis. We found that *pkd2* modulated the localization as well as the activities of SIN. Most notably, *pkd2* promotes a transition to cell growth during cytokinesis, which is opposed by SIN. The role of Pkd2p in cell growth is not limited to cytokinesis. A newly isolated *pkd2* temperature-sensitive mutant blocked the cell size expansion during interphase. Such growth defect was accompanied by frequent cell shrinking, reduced cell volume, and decreased cell stiffness. We conclude that Pkd2p promotes transition to the post-mitosis cell growth in coordination with the Hippo pathway (156 words).

**Introduction:**

Cytokinesis is the last stage of cell division when the two daughter cells separate. During this process, an actomyosin contractile ring assembles at the medial division plane. The ring then provides the mechanical force to drive the cleavage furrow ingression, followed by the separation of the daughter cells. Fission yeast, *Schizosaccharomyces pombe*, is an excellent model organism to study cytokinesis. A large number of cytokinetic mutants have been identified in this model organism. Genetic and cell biology studies have revealed many key components of its cytokinesis, most of which are conserved in metazoans (for a review, see (Pollard and Wu, 2010)).

The fission yeast Hippo pathway SIN plays a central role in the signaling of cytokinesis. The Hippo tumor suppressor pathway consisted of a kinase cascade (for a review see (Yu et al., 2015)), regulates the downstream transcription factors of YAP/TAZ (Huang et al., 2005). It plays essential roles in modulating cell growth and organ size in metazoans (Camargo et al., 2007; Dong et al., 2007). SIN, the fission yeast homologue, consists of more than a dozen essential genes (for reviews, see (Johnson et al., 2012; Simanis, 2015)). At the top of this hierarchy is a GTPase Spg1p, localized at the spindle pole bodies (SPBs) throughout mitosis (Schmidt et al., 1997). Its activation propagates the SIN signal through a cascade of three kinases. At the bottom of the SIN pathway is a nuclear Dbf2-related (NDR) family kinase Sid2p, the homologue of human LATS kinase, which targets many essential cytokinetic proteins (Bohnert et al., 2013; Hergovich, 2016; Sparks et al., 1999; Willet et al., 2019). The activity of SIN in cytokinesis is modulated by MOR (Morphogenesis Orb6 Related), which promotes cell growth through its central component, another NDR kinase Orb6p (Ray et al., 2010; Verde et al., 1998).

Our recent study has identified another essential component of the cytokinetic machinery, the fission yeast homologue of polycystin channels (Morris et al., 2019). Polycystins have been found in both multi-cellular and unicellular eukaryotes since their initial discovery through the genetic studies of one of the most common human genetic disorders, Autosomal Dominant Polycystic kidney disease (ADPKD) (Hughes et al., 1995; Mochizuki et al., 1996). Mutations of human polycystins are the main causes of almost all ADPKD cases, but the mechanism has remained unclear. This has resulted in intensive studies of this family of transmembrane proteins over the last two decades (for recent reviews see (Hardy and Tsiokas, 2020; Ta et al., 2020)). Electrophysiological and structural studies have revealed that most polycystins are calcium-permissive cation channels closely associated with the primary cilium (Gonzalez-Perrett et al.,

2001; Hanaoka et al., 2000; Liu et al., 2018; Su et al., 2018), but their functions have turned out to be surprisingly diverse. While the fruit fly and worm polycystins are essential for the male fertility (Barr and Sternberg, 1999; Watnick et al., 2003), it plays a non-essential structural role in the cilium of green algae *Chlamydomonas reinhardtii* (Huang et al., 2007; Liu et al., 2020; Wood et al., 2012). In comparison, the polycystin homologue of social amoebae *Dictyostelium discoideum* contributes to cell locomotion (Lima et al., 2014). Nevertheless, the mechanism of these cellular functions has remained elusive, including that of human polycystins.

Similar to other unicellular organisms, fission yeast possesses just one homologue of polycystin channel (Palmer et al., 2005). Pkd2p localizes to the plasma membrane in a cell-cycle dependent manner. It concentrates at the cell tips during interphase and the cleavage furrow during cytokinesis (Morris et al., 2019). Knock-down of this essential gene leads to mis-regulation of the contractile ring constriction and failed cell separation (Morris et al., 2019). However, the molecular mechanism underlying the cytokinetic function of Pkd2p remains unclear.

Here we investigated the functional relationship between *pkd2* to SIN during cytokinesis, after discovering their epistatic genetic interaction through a screen. We found that *pkd2* modulated both the localization and activities of SIN. However, *pkd2* opposed SIN most strongly in the transition to cell growth during cytokinesis. Such activity of Pkd2p in promoting growth is further examined through a novel temperature-sensitive *pkd2* mutant that we isolated. Its characterization demonstrated that Pkd2p is equally essential for promoting cell size growth during interphase through maintaining cell stiffness.

**Results:**

## Genetic interactions between SIN and *pkd2* mutants

To understand the role of *pkd2* in the fission yeast cytokinesis, we carried out a genetic screen to identify the interactions between a *pkd2* mutant and a collection of more than thirty cytokinetic mutants. *pkd2-81KD* is a hypomorphic mutant in which the expression of *pkd2* is suppressed by replacing the endogenous promoter with a weak promoter P81nmt1 (Morris et al., 2019). Among the mutants that we examined (Table 1 and Morris et al., 2019), two SIN mutants *sid2-250* and *mob1-R4*, stood out exhibiting the strongest genetic interaction (Morris et al., 2019). The *pkd2* mutation rescued the viability of these two SIN mutants at semi-permissive temperatures. This discovery prompted us to systematically determine the epistatic relationship between *pkd2* and SIN. We examined the genetic interactions between *pkd2-81KD* and seven other SIN mutants (Fig. 1A-B, S1A, and Table 1). Like the *mob1* and *sid2* mutants, three others including *spg1*, *sid4*, and *cdc14* interacted positively with *pkd2-81KD* (Table 1, Fig. 1B), while *cdc7, cdc11,* and *sid1,* showed no genetic interaction (Table 1, Fig. S1A). Unlike the SIN mutants examined above, *cdc16-116* results in hyperactive SIN activities (Fankhauser et al., 1993; Furge et al., 1998). It interacted negatively with *pkd2-81KD* (Fig. 1C). The *pkd2 cdc16* mutant became less viable even at the semi-permissive temperature, compared to the *cdc16* mutant. Combined, our genetic analyses suggested an antagonistic relationship between *pkd2* and the SIN pathway in their regulation of cytokinesis.

Because both Pkd2p and some of the SIN proteins localize to the medial division plane (Morris et al., 2019; Salimova et al., 2000; Sparks et al., 1999), we first tested whether Pkd2p directly regulated the intracellular localization of SIN during cytokinesis. We used quantitative fluorescence microscopy to measure the number of Sid2p and Mob1p molecules throughout cytokinesis. Fission yeast cytokinesis consists of three consecutive stages (i) the contractile ring

assembly and maturation, (ii) the ring constriction, and (iii) the daughter cell separation (Fig. 2A) (Wu et al., 2003). Each lasts ~30 minutes in the wild-type cells at room temperature, relative to the start of prometaphase marked by the separation of spindle pole bodies (SPBs) (Chen and Pollard, 2011; Morris et al., 2019; Wu et al., 2006). As shown before (Goss et al., 2014), both Sid2p-GFP and Mob1p-GFP localized to the medial division plane throughout the stage of ring constriction (Fig. 2B and S1B). They appeared at the division plane ~20 minutes (20') after the separation of SPBs (0'). Their number increased gradually before peaking at 40'. Both eventually dissipated from the medial plane at the end of the ring constriction (60'). In comparison, such kinetics, as well as the numbers of these two molecules at the division plane, remained little changed in the *pkd2-81KD* cells (Fig. 2B and S1B). The only significant difference was that the peak number of Mob1p-GFP molecules increased by 15% in the *pkd2* mutant cells. In addition to the division plane, both Sid2p and Mobp1 also localized to the SPBs throughout cytokinesis. Compared to the wild type, the numbers of these SIN proteins at SPBs almost doubled in the mutant, during the cell separation (60'-90') (Fig 2B, D, S1B). Furthermore, Mob1p-GFP dwelled on the SPBs of the mutant cell much longer (+20 mins) even after cell separation, compared to the wild-type (Fig S1C). We concluded that Pkd2p modulated the cytokinetic localization of Sid2p and Mob1p.

We next determined whether Pkd2p can directly inhibit SIN activities. SIN plays a several essential cytokinetic roles. Here we were focused on its activity in regulating the localization of Cdc7p, septation, and daughter cell integrity.

First, we examined how Pkd2p regulates the asymmetric localization of the SIN pathway kinase Cdc7p (Sohrmann et al., 1998) (Fig. 3A). We measured the dwelling time of Cdc7p-GFP on the two SPBs with time-lapse microscopy. In the wild-type cells, Cdc7p-GFP remained at one

SPB (new) for ~50 minutes, from the start of prometaphase through the end of telophase (Fig. 3A, S1C). In comparison, its localization at the other SPB (old) lasted only ~15 mins (Fig. 3A, S1C), which is consistent with the previous measurements (Dey and Pollard, 2018). We quantified this SIN activity as the ratio of the dwelling times of Cdc7p on the two SPBs (old:new). It averaged ~0.29 in the wild-type cells (Fig. 3B). When SIN is hyperactive, this value would increase to ~1.0 (Dey and Pollard, 2018). In comparison, this SIN activity increased by 33% to 0.38 in the *pkd2* mutant cells (Fig. 3B), mostly as a result of the increased dwelling time of Cdc7p-GFP at the old SPB of the mutant (Fig. S1D). We concluded that *pkd2* slightly modulates the SIN activity as measured by Cdc7p's localization.

Secondly, we examined how Pkd2p regulates the SIN activity of promoting septation. During fission yeast cytokinesis, the formation of septum requires SIN. As shown in many previous studies (Balasubramanian et al., 1998), most SIN mutants failed to form the septum at the restrictive temperature (Fig. 3C). This defect was partially rescued by the *pkd2-81KD* mutation in 6 out of 8 SIN mutants at the restrictive temperature (Fig. 3C). The exceptions were the *cdc7* and *sid1* mutants (Fig. 3C). The most significant effect was found in the *cdc11* mutant, in which septation index increased from 1% to 17% by the *pkd2* mutation. However, many of these septa were thin or partially assembled. We concluded that *pkd2* also modestly modulates the SIN activity measured by septum formation.

Lastly, we tested how Pkd2p regulates the SIN activity of maintaining the integrity of dividing cells. Although less understood, SIN also ensures the integrity of separating cells and prevent their lysis. Consistent with the previous studies (Garcia-Cortes and McCollum, 2009; Gupta et al., 2014; Jin et al., 2006), we found that all SIN mutants lysed at the restrictive temperature, but in varying degrees ranging from 12% (*sid1-125*) to 52% (*cdc14-118*) (Fig. 3D).

The *pkd2-81KD* mutation reduced the fraction of lysed cells to less than 5% for all SIN mutants, except for the *sid1* mutant (Fig. 3D). The lysis of the *cdc14* mutant decreased drastically, by more than 10-folds from 52% to just 3% (Fig. 3D). We concluded that *pkd2* strongly modulates the SIN activity of promoting cell integrity.

Collectively, among the three SIN activities that we measured, *pkd2* opposed SIN most strongly by preventing the daughter cells from lysis. This suggested a model in which *pkd2* promotes the cell size expansion during cytokinesis which is delayed by SIN until mitotic exit. We proceeded to test this model.

**Isolation of a novel *pkd2* temperature-sensitive mutant**

The above results prompted us to isolate new *pkd2* mutants to shed light on Pkd2p's role in cell growth, as the available mutant *pkd2-81KD* exhibited only minor growth defect (Morris et al., 2019). After a screen of the mutants generated through random mutagenesis, we identified a novel temperature-sensitive mutant, *pkd2-B42*. The mutant allele contained eight missense mutations, within the sequence of the transmembrane helices 3-9 (Fig. 4A and Table 2). This mutant was inviable at the restrictive temperature of 36°C or above (Fig. 4B). Such temperature sensitivity was not rescued by the supplementation of sorbitol in the media (Fig. 4C). The mutant was hypersensitive to calcium, similar to the *pkd2-81KD* (Fig. 4D). Most importantly, this mutant grew much slower than either the wild-type or *pkd2-81KD* at the restrictive temperature (Fig. 4E).

The *pkd2-B42* mutant cells exhibited serious morphological and polarity defects. They were significantly shorter and wider than the wild-type cells at the restrictive temperature (Fig. S2A-B). Many of them shrunk at 36°C, distinguished by their reduced size and dense cytoplasm (Fig. 4F). The fraction of such cells increased after extended incubation at 36°C, reaching ~50%

after 8 hours (Fig. 4G). Their actin cytoskeletal structure was marked by a large number of actin patches outside of the growth zones (cell tips or the division plane), unlike that of the wild-type (Fig. S2C). The polarity of this *pkd2* mutant, measured by CRIB-mCherry a fluorescence indicator for active Cdc42p (Tatebe et al., 2008), remained largely unchanged from the wild-type. Active Cdc42p continued to localize to the growth zones in the mutant cells (Fig. S2D). However, in almost half of the mutant cells, the polarity indicator diffused throughout the cytoplasm, a phenotype that was not found in the wild-type cells (Fig. S2D-E). We concluded that this novel temperature-sensitive *pkd2-B42* mutant allele impairs cell morphogenesis.

We next determined whether *pkd2-B42* mutant interacted with the SIN mutants genetically. Like *pkd2-81KD*, *pkd2-B42* exhibited positive interactions with SIN mutants, including those of *sid2, mob1* or *spg1* (Fig. 5A and Fig. S3A). This *pkd2* mutant allele significantly increased the septation indices of both *sid2* and *mob1* mutant cells at the restrictive temperature to 22% and 47% respectively (Fig. 5B). It also reduced the percentage of tetra-nucleated cells, a signature SIN phenotype, from 90% to 7% in *sid2-250* (Fig. S3B). Most impressively, *pkd2-B42* reduced the percentiles of lysed SIN mutant cells to less than 2%, from 17% (*sid2-250*) and 66% (*mob1-R4*) at restrictive temperature (Fig. 5C). Therefore, this novel *pkd2* mutant allele confirmed the antagonism between *pkd2* and SIN during cytokinesis.

The relationship between SIN and *pkd2* bears a strong resemblance to that between SIN and another cell growth promoting pathway MOR, prompting us to investigate the relationship between *pkd2* and MOR. MOR antagonizes SIN during cytokinesis and promotes cell growth (Gupta et al., 2013; Ray et al., 2010; Verde et al., 1998). Similar to the *pkd2* mutants, we found that the MOR mutant *orb6-25* prevented *mob1-R4* from lysis (Fig. 6A). Further, two MOR mutants, *orb6-25* and *mor2-283*, exhibited negative genetic interactions with *pkd2-B42* (Fig.

6B). The morphological defects of *pkd2 MOR* mutants distinguished them from either of the single mutants. MOR mutant cells are spherical or orb-shaped at the restrictive temperature due to its defect in polarized growth (Verde et al., 1998). In comparison, both *orb6 pkd2* and *mor2 pkd2* mutant cells were more similar to the *pkd2* mutant in morphology, without the excessive cell width (Fig. 6D-E). On the other hand, compared to the *pkd2* mutant cells, both *orb6 pkd2* and *mor2 pkd2* mutant cells were more likely to be deflated at the restrictive temperature (Fig. 6F-G). We concluded that *pkd2* and MOR act synergistically, but they have distinct roles in cell morphogenesis.

**The role of *pkd2* in interphase cell growth**

The critical role of Pkd2p in promoting the transition to cell growth during cytokinesis led to our next question, whether it is also required for interphase growth. The rod-shaped fission yeast cells grow exclusively by expanding their tips until reaching the minimum length to enter mitosis, making it an excellent model organism to study this question. We first measured the tip growth of *pkd2-B42* mutant cells using time-lapse microscopy. At the permissive temperature, the mutant cells expanded similarly to the wild-type cells at a rate of ~2 µm/hour (Fig. 7A). However, at the restrictive temperature of 37°C, the expansion of the mutant cells slowed down to a rate of less than 1µm/hour, 4 times lower than the wild-type (Fig. 7A-B, Movie 1 and 2). Time-lapse imaging of the tip expansion revealed that the mutant not only expanded their tips slower but also grew with frequent pauses (66%, n = 229) (Fig. 7B-C), in stark contrast to the wild-type cells. The pause was often accompanied by a temporary shrinkage, distinguished by reduced cellular volume and increased cytoplasmic density, that usually lasted ~20 minutes (16 ± 7 mins, average ± SD, n = 152) (Fig. 7C, Movie S3). The slow tip expansion of *pkd2-B42* cells naturally predicted that it would take much longer for them to reach the minimum length

required for mitotic entry, compared to the wild-type. This hypothesis was confirmed by counting of mitotic cells among the mutant. Less than 1% of *pkd2* mutant cells entered mitosis at the restrictive temperature, far less than that of the wild-type (8%) (Fig. 7D-E). We concluded that Pkd2p also promotes length expansion during interphase growth.

After examining the one-dimensional tip growth, we further investigated the role of Pkd2p in the three-dimensional volume expansion. Although it remains technically challenging to directly measure the volume of a single fission yeast cell, a novel fluorescence microscopy-based approach can do this indirectly (Knapp et al., 2019). The cellular concentration of a constitutively expressed fluorescence protein is used as the indicator of the cell volume. Assuming that biosynthesis of such fluorescence proteins is coupled with cell volume expansion, the fluorescence of yeast cells shall remain constant throughout the cell cycle. However, a defect in volume expansion results in an elevated concentration of the fluorescence protein hence increased intracellular fluorescence (Knapp et al., 2019). We compared the wild-type and *pkd2* mutant cells, both constitutively expressing GFP (super-fold GFP), with quantitative fluorescence microscopy. As expected, the average fluorescence of the wild-type cells clustered close to the average value, in an asynchronous population (Fig. S4A-B). In comparison, the average fluorescence of *pkd2-B42* cells was ~50% higher, exhibiting a bimodal distribution (Fig. S4B). Those temporarily shrunken mutant cells exhibited relatively lower fluorescence compared to the others (Fig. S4B'). We thus confirmed with an alternative method that Pkd2p is required for the size expansion of fission yeast cells.

To understand how Pkd2p promotes cell size expansion, we next tested whether it regulates the turgor pressure that is essential for such growth. As an indirect measurement of the turgor pressure, we quantified cell stiffness with atomic force microscopy (AFM) (Gibbs et al.,

2021). AFM is a scanning probe experimental tool that can provide nanoscale resolution topographical images and characterize the nanomechanical biophysical properties of cellular surfaces (for a review see (Goss and Volle, 2020)). We probed the cells with AFM to acquire force-distance curves of surface indentation and cellular spring constants, indicative of the cellular resistance to the applied force (Fig. 8A-E). Therefore, the spring constant can directly reflect the measure of cell stiffness. The cellular spring constant of wild-type cells (42 ± 10 mN/m, average ± S.D.) was consistent with previously reported values (Gibbs et al, 2021). In comparison, the spring constant of *pkd2-B42* mutant cells was 40% lower at the permissive temperature (26 ± 12 mN/m) (Fig. 8F). It decreased further to 16 ± 11 mN/m at the restrictive temperature, 60% lower than the wild-type (40 ± 12 mN/m) (Fig. 8F). Comparably, the spring constant of the other *pkd2* mutant *pkd2-81KD* was between those of *pkd2-B42* and the wild type. We concluded that *pkd2* is essential for promoting cell stiffness during growth.

## Discussion:

Cytokinesis is often defined as the physical separation of daughter cells, but it also sets the stage to restart the cell growth after mitosis. This growth includes a significant increase in both biomass (Miettinen et al., 2019) and cell volume (Li et al., 2017) during animal cell cytokinesis. Similarly in fission yeast, the cell growth transition is achieved during cytokinesis, evident by the addition of new wall materials and new tip ends for daughter cells. Our study suggests that the conserved polycystin channel Pkd2p is an essential regulator of this transition during cytokinesis.

### Antagonism between SIN and *pkd2* in cytokinesis

The antagonism between *pkd2* and SIN plays out as the cells transit to cell growth during cytokinesis. SIN inhibits such transition through direct inhibition of the MOR pathway (Gupta et al., 2013; Ray et al., 2010). We speculate that with very weak SIN signaling at the restrictive

temperature, the SIN mutant cells restart the cell size growth and lyse as a result. Inhibition of cell growth through *pkd2* mutation thus allows these SIN mutant cells to stay intact and proceed to septation. The *pkd2* mutations may also enhance the residual SIN activity by increasing the cytokinetic localization of SIN proteins, especially at the SPBs. As a result of the antagonism between *pkd2* and SIN, the yeast cells can synthesize the septum and stay intact when both are inhibited.

In contrast to SIN, MOR synergizes with *pkd2*. This NDR kinase Orb6p mediated pathway shares striking similarities to Pkd2p, besides their common antagonism towards SIN. MOR and Pkd2p exhibit similar localization at the growth zones where they both promote growth. Like Pkd2p, Orb6p and other MOR pathway proteins localize to the cell tip during interphase and to the division plane during cytokinesis (Hirata et al., 2002; Hou et al., 2003; Verde et al., 1998). However, Pkd2p and MOR also differ from each other in two important ways. While MOR regulates the Cdc42p-mediated cell polarity pathway (Das et al., 2009; Tay et al., 2019), *pkd2* does not. MOR is only required for tip growth, but *pkd2* is essential for cell growth regardless of the polarity. We propose that Pkd2p is downstream from MOR in a signaling network that regulates cell size growth and their functions do not completely overlap.

Pkd2p may not be alone in suppressing SIN during cytokinesis through its promotion of cell growth. Genetic screens have identified quite a number of SIN suppressors which include *ace2, dnt1, scw1, sec8, ypa1, ypa2* , and *zfs1* (Beltraminelli et al., 1999; Goyal and Simanis, 2012; Jin and McCollum, 2003; Jin et al., 2007; Jin et al., 2006; Karagiannis et al., 2002; Ray et al., 2010). They play a variety of molecular functions including exocytosis, RNA binding, and mitotic progression. Although it remains unclear how they interact with SIN, we propose that

many of these suppressors may share a role with Pkd2p in promoting the cell growth transition during cytokinesis.

**The role of Pkd2p in the cell size regulation**

Collectively, our data support a model that Pkd2p regulates the homeostasis of intracellular osmolarity to promote cell size growth. In fission yeast as in other fungi, the difference between the intracellular and extracellular osmolarity is essential to maintain the turgor pressure required for cell tip expansion (Lew, 2011; Minc et al., 2009). Both the *pkd2* mutants, *pkd2-81KD* and *pkd2-B42*, exhibit a defect in maintaining cellular volume regardless of their cell-cycle stage (Morris et al., 2019). Although we have not directly measured the turgor pressure of these mutant cells, their decreased stiffness (Arfsten et al., 2010; Arnoldi et al., 2000), temporary shrinkage, and reduced cell volume are most likely due to a defect in regulating the intracellular osmolarity that is essential to maintain the cell size.

Although the cell wall is equally important for fission yeast cell growth, we have so far found no evidence to support an alternative model that Pkd2p is directly required for cell wall biosynthesis. In contrast to most cell wall mutants, the cell wall structure of the *pkd2* mutant cells is similar to that of the wild-type cells (Morris et al., 2019). Further, unlike the mutants of cell wall biosynthesis, *pkd2* mutants cannot be rescued by sorbitol. While the cell wall mutants frequently lysed during cell separation (Cortes et al., 2012; Munoz et al., 2013), the *pkd2* mutant cells underwent reversible shrinkage but rarely lysed. Interestingly, our study of the *pkd2* mutants also reveals that the cell wall of fission yeast is flexible enough to recover from significant shrinking. Such flexibility is similar to the cell wall of both plants and bacteria.

Pkd2p likely promotes the cell size growth as a mechanosensitive channel either by directly regulating ion homeostasis or by regulating the calcium signaling pathway. Although the

electrophysiology study of Pkd2p is lacking, indirect evidence including its sensitivity to channel blockers points to its likely activity as an ion channel (Aydar and Palmer, 2009). Pkd2p may directly regulate the ion homeostasis of potassium or sodium to regulate the intracellular osmolarity. The human polycystin-2 channel allows the passage of both cations (Liu et al., 2018). However, we prefer a model in which Pkd2p regulates the calcium influx to regulate the calcium signaling. It is more consistent with the critical role of calcium in regulating the intracellular osmolarity of fission yeast (Ma et al., 2011; Poddar et al., 2021). Such a model would also agree with the importance of the calcium-signaling molecules calcineurin and calmodulin in fission yeast cytokinesis (Moser et al., 1997; Yoshida et al., 1994).

The role of Pkd2p in promoting cell growth is likely conserved. Pkd2p homologues can be found among many fungi species and they constitute one of seventeen essential fungal protein families (Hsiang and Baillie, 2005). Similar to Pkd2p, Spray of *Neurospora crassa* promotes the tip growth of this filamentous fungus (Bok et al., 2001; Stephenson et al., 2014). It is presumed to regulate the calcium influx and maintain a calcium gradient at the expanding hyphal (Silverman-Gavrila and Lew, 2003). The other Pkd2p homologues included FlcA/B/C of Aspergillus fumigatus (de Castro et al., 2017) and CaFlc1-3 of Candida albicans (Protchenko et al., 2006). Four homologues of Pkd2p have been identified in *Saccharomyces cerevisiae*, but none of them is essential and their function in cell growth has not been examined (Protchenko et al., 2006; Rigamonti et al., 2015). Compared to fungi, the role of polycystins in the cell growth of other eukaryotes remains ambiguous. Its interaction with the Hippo pathway has only been examined recently. Increased activity of the Hippo effector YAP was found in the polycystin mutant kidney cells (Cai et al., 2018).

In summary, our study reveals the importance of the transition to cell growth regulated jointly by the Polycystin channel Pkd2p and the Hippo pathway SIN during cytokinesis.

## Materials and Methods:

### Yeast genetics

Yeast cell culture and genetic procedures were carried out according to the standard methods. We used YE5s media for growing the cells. A SporePlay+ dissection microscope (Singer, England) was used for tetrad dissection and developing different strains. For viability assays, we inoculated the cells in liquid YE5s media at 25°C overnight before setting up the ten-fold dilution series on YE5S agar plates. The plates were incubated at designated temperatures for two days before being imaged using a photo scanner (Epson).

### Identification of temperature-sensitive *pkd2* mutant

To isolate *pkd2* temperature-sensitive mutants, we adopted the approach of marker reconstitution mutagenesis (Tang et al., 2011) with some modifications. We first amplified the DNA fragment coding for C-terminal truncated His5 (His5CterΔ) and *ura4* from pH5C vector (Tang et al., 2011) through PCR using primers P602 and P603 (Table 3). The primers include sequences homologous to the 3'UTR of *pkd2*. The amplified DNA fragment was transformed into yeast using the lithium acetate method. The resulting yeast strain (QCY-999) was selected on EMM plates without uracil supplement, and also confirmed through PCR and Sanger sequencing. Next, the coding sequence of *pkd2* including its 3'UTR was cloned into the vector pH5D (Tang et al., 2011) which contains the missing C-terminal fragment of His5 (His5Cter). The resultant vector (QCV-193) was used as the template to perform random mutagenesis of *pkd2* through error-prone PCR. The reaction used for random mutagenesis included Taq DNA polymerase (NEB) in

the presence of 200µM $MnCl_2$ (Sigma). The mutated *pkd2* together with the sequence of His5Cter (PCR product) were transformed into the strain (QCY-999) to replace the wild-type gene at its endogenous locus. The transformants were selected on EMM plates without histidine supplement. The positive clones were further screened for temperature sensitivity through incubation on YE5s supplemented with Phloxin B at 36°C for two days. The temperature-sensitive mutants were isolated and back-crossed with the wild-type twice to confirm their phenotype. The ORF sequence of the *pkd2-B42* mutant was amplified through PCR and sequenced through the Sangers method to identify the point mutations.

**Microscopy**

For all microscopy experiments, the cells were inoculated in liquid YE5s media (unless specified) at 25°C for two days before being harvested during the exponential growth phase at a density between 5 x $10^6$/ml and 1.0 x $10^7$/ml. For temperature sensitive mutants, exponentially growing cell cultures were temperature shifted for 4 hours unless mentioned otherwise before live imaging or fixation.

For time lapse fluorescent microscopy and live cell still microscopy, following temperature shift cells were harvested by centrifugation at 4,000 rpm for 1 minute. Concentrated re-suspended cells were applied to a pad (YE5s + 25% gelatin). The samples were sealed under the coverslip with VALAP (a mix of an equal amount of Vaseline, lanolin, and paraffin) and imaged.

We used a spinning disk confocal microscope equipped with an EM-CCD camera for fluorescence microscopy. The Olympus IX71 microscope was equipped with the objective lenses 100x (NA = 1.40, oil), 60x (NA = 1.40, oil) and 40x (1.30, oil), a confocal spinning disk unit (CSU-X1, Yokogawa, Japan), a motorized XY stage and a Piezo Z Top plate (ASI, USA). Solid-

state lasers of 405 nm, 488 nm, or 556 nm were used at a power of no more than 5 mW (< 10%). The images were acquired by an Ixon-897 camera controlled by iQ3.0 (Andor, Ireland). We imaged cells by acquiring 15 slices at a step size of 0.5 µm for Z-series or 8 slices at a step size of 1 µm. Most time-lapse microscopies were done at the room temperature maintained at around 23°C. To minimize the temperature variations, we undertook microscopy of both the wild-type and mutants on the same or consecutive days.

For time-lapse microscopy to capture the tip growth, 20 µl of exponentially growing cell culture was spotted onto a glass coverslip (#1.5) in a 10 mm petri dish (Cellvis, USA). The coverslip was precoated with 50 µl of 50 µg/ml lectin (Sigma, L2380) which was allowed to dry overnight at 4°C. The cells were overlaid with a 9 mm diameter YE5s agar block (~ 5 mm height), dish covered, and imaged. To measure the tip growth at the restrictive temperature, time lapse microscopy was performed using an Olympus IX81 microscope enclosed in a temperature-controlled chamber (Precision Control). Additionally, exponentially growing cells were first temperature shifted in liquid culture at 36°C for 4 hours. Following mounting in petri-dish as above, they were immediately imaged in the pre-equilibrated chamber. Brightfield images were acquired with a 60x oil objective lens (Olympus, NA=1.42) and a CoolSNAP HQ2 camera (Photometrics) with 1 X 1 binning. For measuring growth rate at room temperature, the spinning disk confocal microscope mentioned was used.

To measure the septation and mitotic indices, the calcofluor, and DAPI stained cells were imaged with an Olympus IX81 microscope equipped with 60x oil lens (NA=1.42) and a digital camera C11440 (Hamamatsu, Japan). Images were acquired using CellSens (Olympus). Brightfield images were illuminated with LED lamp. For visualizing the cell wall, cells were fixed with 4% paraformaldehyde (Fisher), washed with TEMK buffer, and stained cells with

1µg/ml of calcofluor (Sigma). For nuclear staining, cells were fixed with 70% cold ethanol and stained with 1µg/ml DAPI (Sigma). For some septation indices measurement, the spinning disk confocal microscope with 40x oil objective was used. Laser at 405nm was used at 1% with 25 m/s exposure.

**Image analysis**

We used Image J (NIH) to process all the microscopy images, with either freely available or customized macros/plug-ins. For quantitative analysis, the fluorescence micrographs were corrected for both X-Y driftings by StackReg plug-in (Thevenaz et al., 1998) and photo-bleaching by EMBLTools plug-in (Rietdorf, EMBL Heidelberg). Unless specified, the sums of all Z-slices were used for quantification. All the measurements were corrected with background subtraction.

The SPB localization of Cdc7p-GFP, Sid2p-GFP, and Mob1p-GFP was quantified by measuring the total fluorescence in a 0.8 µm by 0.8 µm (8 by 8 pixels) circle. The background fluorescence was the fluorescence intensities in a ring of 1µm (12 x 12 pixel) surrounding the circle. The contractile ring localization of Sid2p-GFP and Mob1p-GFP was quantified by measuring the fluorescence in a 3-4µm by 0.8 µm (30-40 by 8 pixels) rectangle centering on the cell division plane. The background fluorescence was the fluorescence intensity in 3-4 µm by 0.2 µm rectangle (30-40 by 2 pixels) adjoined to the division plane on both sides.

All the figures have been made with Canvas (ACD Systems) and the plots were created using Origin (OriginLab) and KaleidaGraph.

**Atomic Force Microscopy imaging and analysis of cells**

Yeast strains were cultured in YE5S medium at 25°C in the mid-log phase ($OD_{595}$ < 0.6) for 36 hours prior to imaging. For restrictive temperature experiments, cells were shifted to 36°C for 8 hours. Cells for AFM imaging and analysis were centrifuged at 500g and washed with EMM5S medium prior to plating on plastic dishes. Plastic dishes were prepared for yeast cell adhesion by plasma cleaning with PDC-32G plasma cleaner (Harrick Plasma, Ithaca, NY) for 3 minutes followed by incubation for 48 hours at 4°C with 0.8 mg/mL CellTak adhesive (Corning Life Sciences, Glendale, AZ) diluted in 0.1M $NaHCO_3$. Dishes were washed twice with $ddH_2O$ to remove excess CellTak prior to plating cells. Yeast cells were added to the dish and centrifuged at 500g for 20 seconds using a swinging bucket rotor. Non-adherent cells were removed by three EMM5S washes and aspiration.

Topographical height and deflection AFM images were obtained in contact mode using an MFP-3D AFM (Asylum Research, Santa Barbara, CA). Silicon Nitride AFM pyramidal tip PNP-TR probes (Nanoworld, Neuchatel, Switzerland) with a nominal spring constant of 0.32 N/m were used for all experiments. Cells were maintained in EMM5S media throughout AFM imaging and analysis to prevent drying out. 2D images were exported from MFP-3D software and scale bars were added in Adobe Photoshop. Following topographical imaging, force data was obtained from yeast cells at a deflection set point of 4nN to minimize damage to the cell surface. Ten representative points were selected along the length of each cell, and ten force curves were obtained at each location, for a total of 100 force curves per cell. The extension force curve representing the tip approach and contact with the surface was used to calculate the spring constant for the surface. The spring constants ($k_{cell}$) were calculated from the linear region of the extension curve using a two-spring model with the equation:

$$\frac{1}{keffective} = \frac{1}{kcell} + \frac{1}{kcantilever}$$

where $k_{cantilever}$ was experimentally calculated using the thermal tuning method (Hutter and Bechhoefer, 1993), and the slope of the extension force curve linear region is $k_{effective}$ (Volle et al., 2008). Data processing was performed through MFP-3D software in Igor Pro to obtain curve fits and spring constants.

**Acknowledgement**

QC conceptualized the study, DS, JG, and QC designed the experiments, DS, DI, EG, MC, JG, and QC carried out the experiments, DS, DI, EG, MC, JG, and QC analyzed the data, DS, JG, and QC wrote the manuscript. The authors thank Abhishek Poddar and Mamata Malla for their technical support. The authors thank Mohan Balasubramanian (University of Warwick, UK), Daniel McCollum (University of Massachusetts Medical School), Jian-Qiu Wu (Ohio State University) and Pilar Perez (University of Salamanca, Spain) for sharing yeast strains and plasmids with us. We acknowledge the National Bio Resources Project – Yeast Base (Japan) for sending yeast strains. We would like to thank the group of Song-Tao Liu for sharing their microscope. This work has been supported by the University of Toledo startup fund (QC), National Institutes of Health grant R15GM134496 (QC), DeArce-Koch Memorial Fund (QC), University of Toledo Undergraduate Summer Research and Creative Activities Program (DI), Wellesley College startup fund (JG), and National Science Foundation grant DBI1528288 (JG). The content is solely the responsibility of the authors and does not necessarily represent the official views of the National Institutes of Health.

**Table 1: Genetic interaction of *pkd2* mutants and selected cytokinetic mutants**

| Gene | Mutant | Genetic interactions |
|---|---|---|
| *ace2* | *ace2Δ* | - |
| *agn1* | *agn1Δ* | *No* |
| *ags1* | *mok1-664* | *No* |
| *bgs4* | *cwg1-2* | *No* |
| *cdc11* | *cdc11-123* | *No* |
| *cdc14* | *cdc14-118* | ++ |
| *cdc16* | *cdc16-116* | -- |
| *cdc42* | *cdc42-1625* | *No* |
| *cdc7* | *cdc7-24* | *No* |
| *eng1* | *eng1Δ* | *No* |
| *exo70* | *exo70Δ* | - |
| *far8* | *far8Δ* | *No* |
| *mid1* | *mid1Δ* | *No* |
| *mid2* | *mid2Δ* | *No* |
| *mor2* | *mor-282* | -- |
| *myp2* | *myp2Δ* | *No* |
| *orb6* | *orb6-25* | -- |
| *rga7* | *rga7Δ* | *No* |
| *rgf1* | *rgf1Δ* | *No* |
| *rgf2* | *rgf2Δ* | *No* |
| *sid1* | *sid1-125* | ++ |
| *sid4* | *sid4-A1* | + |
| *spg1* | *spg1-106* | ++ |
| *sty1* | *sty1Δ* | *No* |

A summary of the genetic interaction between *pkd2* mutants and other gene mutants based on cell viability assay. Positive interactions are designated by either "++" (strong) or "+" (weak) and negative interactions are designated by either "--" (strong) or "- "(weak), No designates no interactions.

472 **Table 2: List of mutations in *pkd2-B42***

| Residue | TMHs | Mutation | Amino acid Nature |
|---|---|---|---|
| 335 | 3rd | F → S | Hydrophobic to Polar |
| 408 | 5th | S → P | Polar to Polar |
| 521 | Between 7th and 8th | N → D | Polar to Polar |
| 530 | 8th | M → V | Hydrophobic to Hydrophobic |
| 534 | 8th | S → G | Polar to Polar |
| 543 | 8th | Q → E | Polar to Charged |
| 555 | 9th | I → T | Hydrophobic to Polar |
| 571 | 9th | I → T | Hydrophobic to Polar |

473

474 **Table 3: List of primers**

| | |
|---|---|
| QC-P596 | *AGAGTCGAATTTTATTGATG* |
| QC-P597 | *ATGCCGCATAGTTAAGCCAG* |
| QC-P598 | *GTCGTTCTTTTCCTGACATA* |
| QC-P599 | *TATGTCAGGAAAAGAACGAC* |
| QC-P600 | *CTGAAGTCCCAAGCACGAAG* |
| QC-P601 | *CTTCGTGCTTGGGACTTCAG* |
| QC-P602 | *ACGTTTATTAACATTTTATTGAAACAATCTATAGACACCGGTAAGAATAAATCCATAAGCCAT TCCCAAA-GGAAATAGTAAGGCTAGTAG* |
| QC-P603 | *GAATATATGCCTATTCGCAATCTAGAATTCCTTTGAATACACCCAATTACAAGCTTAAACGAT TCGGTAT-TAAAAATAGGCGTATCACGAGG* |
| QC-P604 | *AGCATATTTGTTGGATGTGC* |
| QC-P605 | *AA-CGATCG-ATGAGGCTTTGGAGAAGCCCAC* |
| QC-P606 | *AA-GGATCC-TTTGGGAATGGCTTATGGATTTATTC* |
| QC-P607 | *GACGAAGCTCTTTCTAGAAGCGTAGT* |

475

476 **Table 4: List of yeast strains**

| Strain number | mating type | Genotype | Source |
|---|---|---|---|
| FY527 | *h-* | *leu1-32 ura4-D18 his3-D1 ade6-M216* | Lab stock |
| FY528 | *h+* | *leu1-32 ura4-D18 his3-D1 ade6-M210* | Lab stock |
| QC-Y569 | *h-* | *cdc11-123* | Lab stock |
| QC-Y570 | *h-* | *sid4-A1* | Lab stock |
| QC-Y571 | *h+* | *spg1-106* | Lab stock |
| QC-Y573 | *h+* | *cdc16-116* | Lab stock |
| QC-Y574 | *h-* | *cdc7-24* | Lab stock |
| QC-Y576 | *h+* | *sid2-250* | Lab stock |
| QC-Y577 | *h-* | *mob1-R4* | Lab stock |
| QC-Y624 | *h+* | *cdc14-118* | Lab stock |
| QC-Y670 | *h-* | *myp2::kanMX6* | Lab stock |
| QC-Y675 | *h-* | *mob1-mEGFP-kanMX6* | Lab stock |
| QC-Y676 | *h-* | *sid2-mEGFP-kanMX6* | Lab stock |
| QC-Y723 | *h+* | *sid1-125 ura4-D18 leu1-32 ade6-210* | Lab stock |
| QC-Y725 | *h+* | *ace2::kanR ura4-D18 ade6-216 leu1-32 h+* | Lab stock |
| QC-Y743 | *h+* | *far8::kanMX6* | Bioneer |
| QC-Y803 | *h-* | *orb6-25* | Lab stock |
| QC-Y810 | *h-* | *KanMX6-P81nmt1-pkd2 leu1-32 ura4-D18 his3-D1* | Lab stock |
| QC-Y817 | *h+* | *kanMX6-81xnmt1-pkd2 leu1-32 ura4-D18 his3-D1 ade6-M?* | Lab stock |
| QC-Y874 | *h-* | *sty1::kanMX6* | Lab stock |
| QC-Y930 | *h?* | *kanMX6-81xnmt1-Pkd2 sid2-mEGFP-kanMX6* | This study |
| QC-Y933 | *h?* | *kanMX6-81xnmt1-Pkd2 mob1-mEGFP-kanMX6* | This study |
| QC-Y976 | *h?* | *kanMX6-81xnmt1-pkd2 cdc16-116* | This study |
| QC-Y977 | *h?* | *kanMX6-81xnmt1-pkd2 cdc14-118* | This study |
| QC-Y978 | *h?* | *kanMX6-81xnmt1-pkd2 cdc11-123* | This study |
| QC-Y979 | *h?* | *kanMX6-81xnmt1-pkd2 spg1-106* | This study |
| QC-Y980 | *h?* | *kanMX6-81xnmt1-pkd2 sid4-A1* | This study |
| QC-Y983 | *h?* | *kanMX6-81xnmt1-pkd2 cdc7-24* | This study |
| QC-Y986 | *h-* | *ade5D ade7::Ade5 his5D leu1-32 ura4D-18* | MBY6218 (Mohan Balasubramanian) |
| QC-Y999 | *h-* | *pkd2-3'UTR-his5CterD-ura4* | This study |
| QC-Y1010 | *h+* | *mid1::kanMX6* | Bioneer |
| QC-Y1011 | *h+* | *mid2::kanMX6* | Bioneer |
| QC-Y1012 | *h+* | *rga7::kanMX6* | Bioneer |
| QC-Y1013 | *h+* | *rgf1::kanMX6* | Bioneer |
| QC-Y1017 | *h?* | *kanMX6-81xnmt1-pkd2 myp2::kanMX6* | This study |
| QC-Y1017 | *h?* | *kanMX6-81xnmt1-pkd2 myp2::kanMX6* | This study |
| QC-Y1022 | *h?* | *kanMX6-81xnmt1-pkd2 mid1::kanMX6* | This study |
| QC-Y1023 | *h?* | *kanMX6-81xnmt1-pkd2 mid2::kanMX6* | This study |
| QC-Y1024 | *h?* | *kanMX6-81xnmt1-pkd2 rga7::kanMX6* | This study |
| QC-Y1025 | *h?* | *kanMX6-81xnmt1-pkd2 rgf1::kanMX6* | This study |

| | | | |
|---|---|---|---|
| QC-Y1031 | *h-* | *pkd2::pkd2-B42-ura4+-his5+ leu1-32* | This study |
| QC-Y1032 | *h+* | *pkd2::pkd2-B42-ura4+-hist5+ leu1-32* | This study |
| QC-Y1032 | *h+* | *pkd2::pkd2-B42-ura4+-hist5+ leu1-32* | This study |
| QC-Y1036 | *h?* | *pkd2::pkd2-B42-ura4+-his5+ leu1-32 sid2-250* | This study |
| QC-Y1037 | *h?* | *pkd2::pkd2-B42-ura4+-his5+ leu1-32 mob1-R4* | This study |
| QC-Y1061 | *h+* | *eng1:: KanMx6* | Bioneer |
| QC-Y1062 | *h+* | *rgf2::kanMX6* | Bioneer |
| QC-Y1066 | *h-* | *mok1-664* | JW7572(Jian-Qiu Wu) |
| QC-Y1067 | *h?* | *cwg1-2* | JW7551(Jian-Qiu Wu) |
| QC-Y1070 | *h-* | *ura4::Pact-sfGFfP-ura4* | This study |
| QC-Y1072 | *h?* | *pkd2::pkd2-B42-ura4+-his5+ leu1-32 far8::kanMX6* | This study |
| QC-Y1073 | *h?* | *kanMX6-81xnmt1-pkd2 far8::kanMX6* | This study |
| QC-Y1080 | *h?* | *pkd2::kanMX6-81xnmt1-pkd2 ura4::Pact-sfGFfP-ura4* | This study |
| QC-Y1081 | *h?* | *eng1:: KanMx6 pkd2::pkd2-B42-ura4+-his5+ leu1-32* | This study |
| QC-Y1082 | *h?* | *rgf2:: KanMx6 pkd2::pkd2-B42-ura4+-his5+ leu1-32* | This study |
| QC-Y1085 | *h?* | *eng1:: KanMx6 kanMX6-81xnmt1-pkd2* | This study |
| QC-Y1093 | *h?* | *pkd2::pkd2-B42-ura4+-his5+ leu1-32 mok1-664* | This study |
| QC-Y1096 | *h?* | *mok1-664 KanMX6-81xnmt1-pkd2* | This study |
| QC-Y1108 | *h?* | *cwg1-2 pkd2::pkd2-B42-ura4+-his5+ leu1-32* | This study |
| QC-Y1109 | *h?* | *cwg1-2 kanMX6-81xnmt1-pkd2* | This study |
| QC-Y1129 | *h+* | *cdc7-GFP::ura4* | MBY2415 (Mohan Balasubramanian) |
| QC-Y1154 | *h?* | *kanMX6-81xnmt1-pkd2 leu1-32 cdc7-GFP::ura4* | This study |
| QC-Y1162 | *h+* | *agn1::kanMX6* | Bioneer |
| QC-Y1168 | *h?* | *KanMX6-81xnmt1-pkd2 sid1-125 leu1-32 ade6-210* | This study |
| QC-Y1178 | *h?* | *KanMX6-81xnmt1-pkd2 ace2::kanR* | This study |
| QC-Y1181 | *h?* | *agn1::kanMX6 pkd2::pkd2-B42-ura4+-his5+ leu1-32* | This study |
| QC-Y1190 | *h?* | *agn1::kanMX6 kanMX6-81xnmt1 pkd2* | This study |
| QC-Y1198 | *h?* | *orb6-25 pkd2::pkd2-B42-ura4+-his5+ leu1-32* | This study |
| QC-Y1208 | *h-* | *cps212-282 or mor2-282* | FY13846 (CP28-2) NBRP Japan |
| QC-Y1212 | *h-* | *his5+:pact1:CRIB[gic2aa1-181]-3mCherry:bsdMX* | FY38515 (AV2324) NBRP Japan |
| QC-Y1227 | *h?* | *pkd2::pkd2-B42-ura4+-his5+ leu1-32 his5+:pact1:CRIB[gic2aa1-181]-3mCherry:bsdMX* | This study |
| QC-Y1250 | *h+* | *mor2-282 (cps12-282) pkd2::pkd2-B42-ura4+-his5+ leu1-32* | This study |
| QC-Y1254 | *h?* | *exo70Δ::kanMX6* | This study |
| QC-Y1256 | *h?* | *pkd2::pkd2-B42-ura4+-his5+ leu1-32 exo70Δ::kanMX6* | This study |
| QC-Y1265 | *h?* | *orb6-25 sid2-250* | YDM4254(Daniel McCollum) |
| QC-Y1266 | *h?* | *orb6-25 mob1-R4* | YDM4341(Daniel McCollum) |
| QC-Y1274 | *h?* | *pkd2::pkd2-B42-ura4+-his5+ leu1-32 spg1-106* | This study |
| QC-Y1290 | *h+* | *leu1-32 ura4-D18 cdc42-1425:kanMX6* | PPG5660(Pilar Perez) |
| QC-Y1307 | *h?* | *cdc42-1625 pkd2::pkd2-B42-ura4+-his5+ leu1-32* | This study |
| QC-Y1352 | *h?* | *sty1::kanMX6 pkd2::pkd2-B42-ura4+-hist5+ leu1-32* | This study |

477

## Figures and Figure legends:

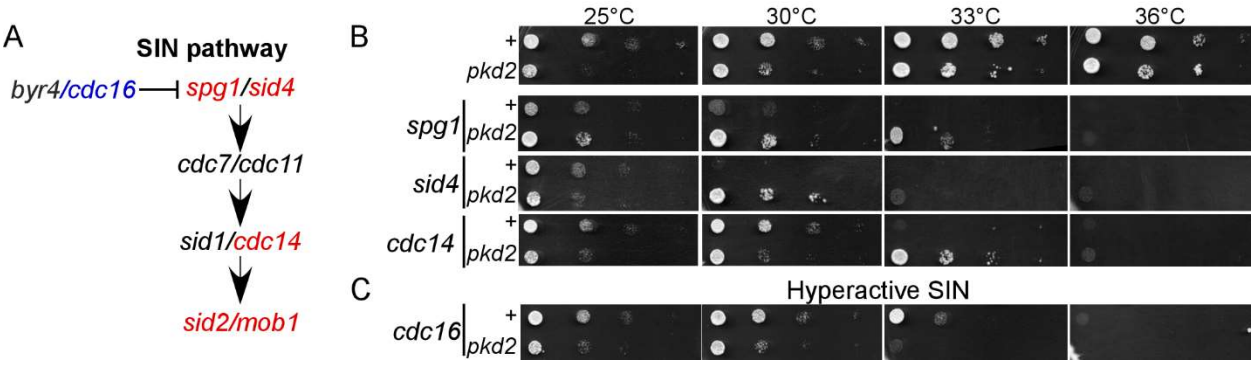


**Figure 1. The epistatic genetic interaction between *pkd2* and SIN.**

**(A)** A diagram of the SIN pathway. The genes mutants which have been tested are colored in either blue (negative interaction) or red (positive interaction)

**(B)** Ten-fold dilution series of designated strains at the indicated temperatures.

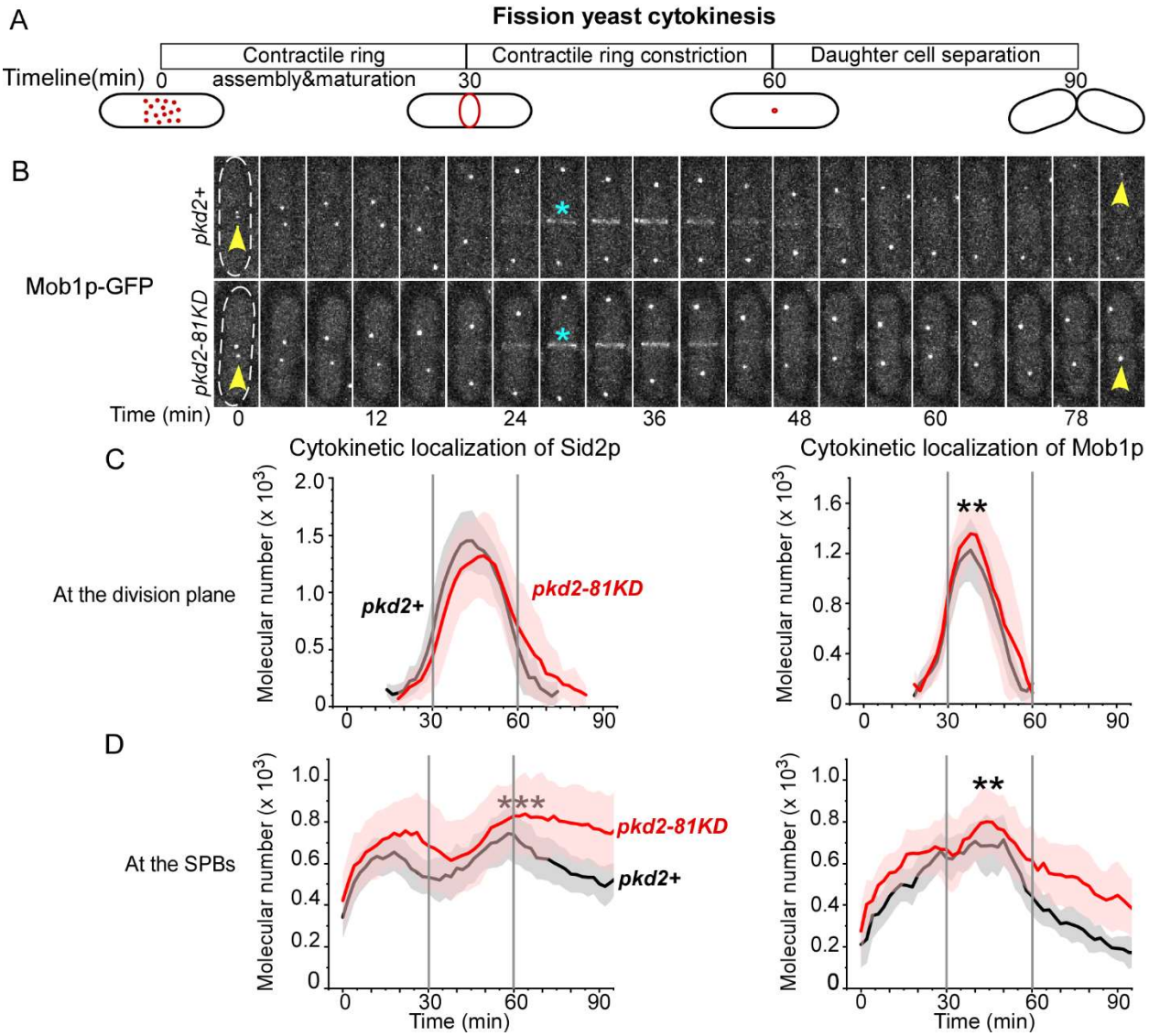


**Figure 2. Localization of SIN proteins in the *pkd2* mutant during cytokinesis.**

**(A)** Scheme showing the key events of cytokinesis in fission yeast: contractile ring assembly, ring constriction, and daughter cell separation with respect to the average timeline of the wild-type cells at 25°C. Time zero denotes the separation of SPBs during prometaphase.

**(B)** Time-lapse micrographs of either a wild-type (top) or a *pkd2-81KD* (bottom) cell expressing Sid2p-GFP. Number denotes time in minutes after SPB separation. Interval = 4minutes. Arrowhead: SPB separation, Asterisk*: Appearance of Sid2p-GFP at the division plane.

**(C-D)** Time-courses of the number of Sid2p-GFP (left) or Mob1p-GFP (right) molecules in the division plane (C) and in SPB (D) of either wild-type (black line) or the *pkd2* mutant (red line). The data was pooled from two independent biological repeats (n>20). Mob1p molecular number increased in the division plane. **: $P < 0.01$, ***: $P < 0.001$.

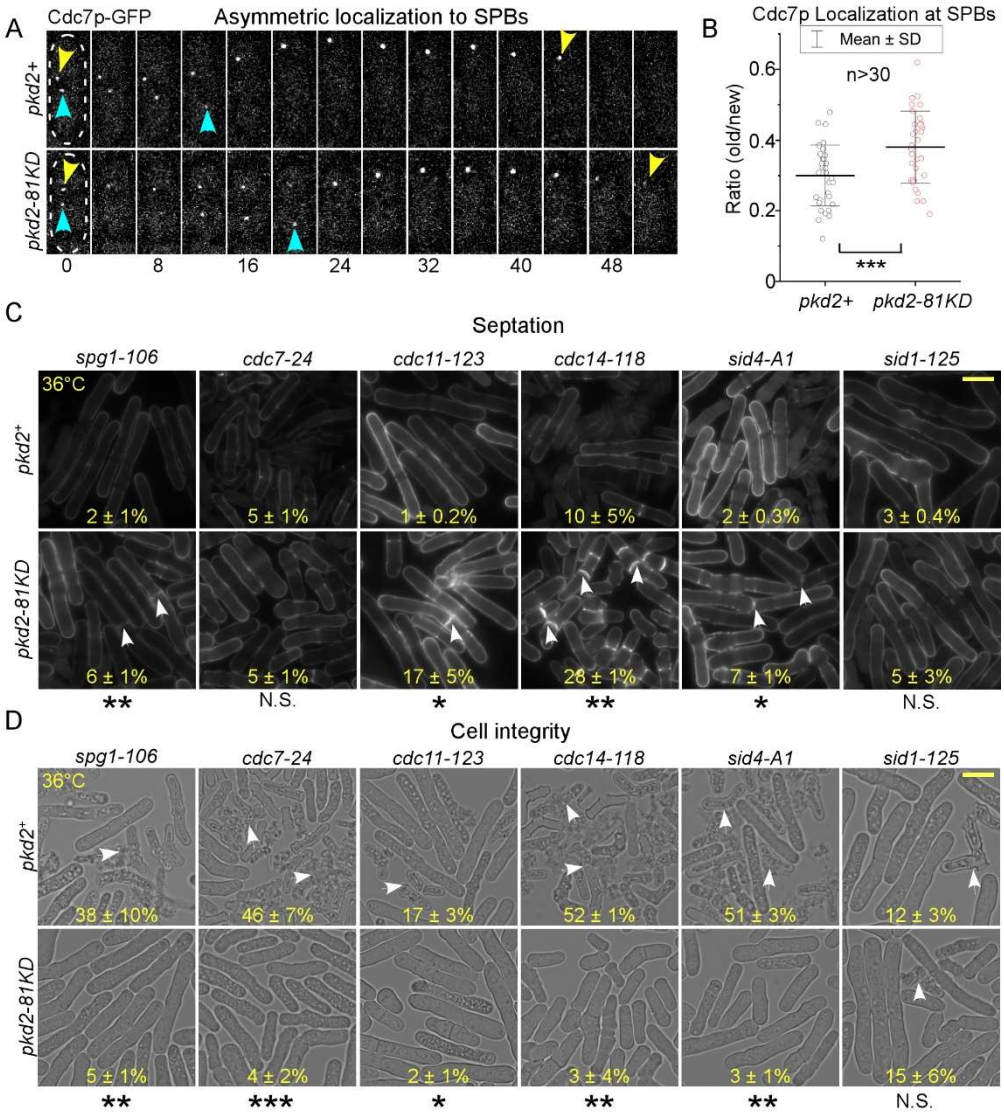


**Figure 3. Depletion of Pkd2p altered SIN asymmetry, rescued septation, and prevented lysis of the SIN mutant cells.**

**(A-B)** Asymmetric distribution of the SIN protein Cdc7p to the two SPBs. (A) Time-lapse micrographs of either a wild-type (top) or a *pkd2* mutant (bottom) expressing Cdc7p-GFP. Time zero represents the time point of SPBs separation. Arrowheads denote new (yellow), and old (blue) SPB. (B) Dot plots showing ratio of the dwelling time (old/new) of Cdc7p at the SPBs. The data was pooled from two independent biological repeats n>30.

**(C)** Fluorescence micrographs of either SIN (top) or *pkd2-81KD* SIN (bottom) mutants fixed and stained with calcofluor to visualize septum.

**(D)** Bright-field micrographs of the SIN (top) and SIN *pkd2* mutant (bottom) cells at the restrictive temperature of 36°C. The numbers represent the percentage of septated or lysed cells (average ± standard deviations). Arrow heads point to the septated (C) or lysed (D) cells. The data was pooled from at least two independent biological repeats (n > 400). Scale bar represents length of 10μm. *:P<0.05, **:P<0.01, ***: P<0.001

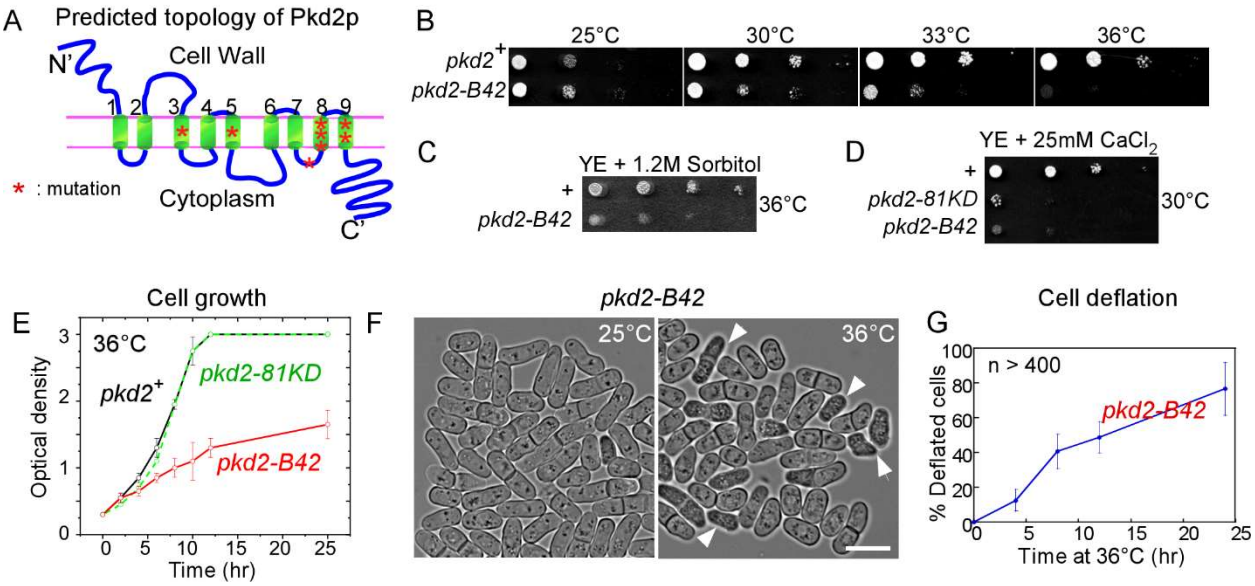


**Figure 4. A novel temperature-sensitive *pkd2* mutant.**

**(A)** Scheme showing predicted topology of the wild-type Pkd2p. The mutated residues in *pkd2-B42* are shown in red asterisks. Numbers denote each transmembrane helix. All eight mutations are in the transmembrane domains.

**(B-D)** Ten-fold dilution series of yeast cells at indicated temperatures and conditions.

**(E)** The growth curve of the wild-type (black line), *pkd2-81KD* (green) and *pkd2-B42* (red) cells at 36°C. Error bars represent standard deviations.

**(F)** Bright-field micrographs of the *pkd2-B42* cells at permissive 25°C (left) and restrictive temperature of 36°C (right).

**(G)** Time course of the percentage of the deflated cells. The data was pooled from at least two independent biological repeats (n > 300). Error bars represent standard deviations. Scale bar represents length of 10μm.

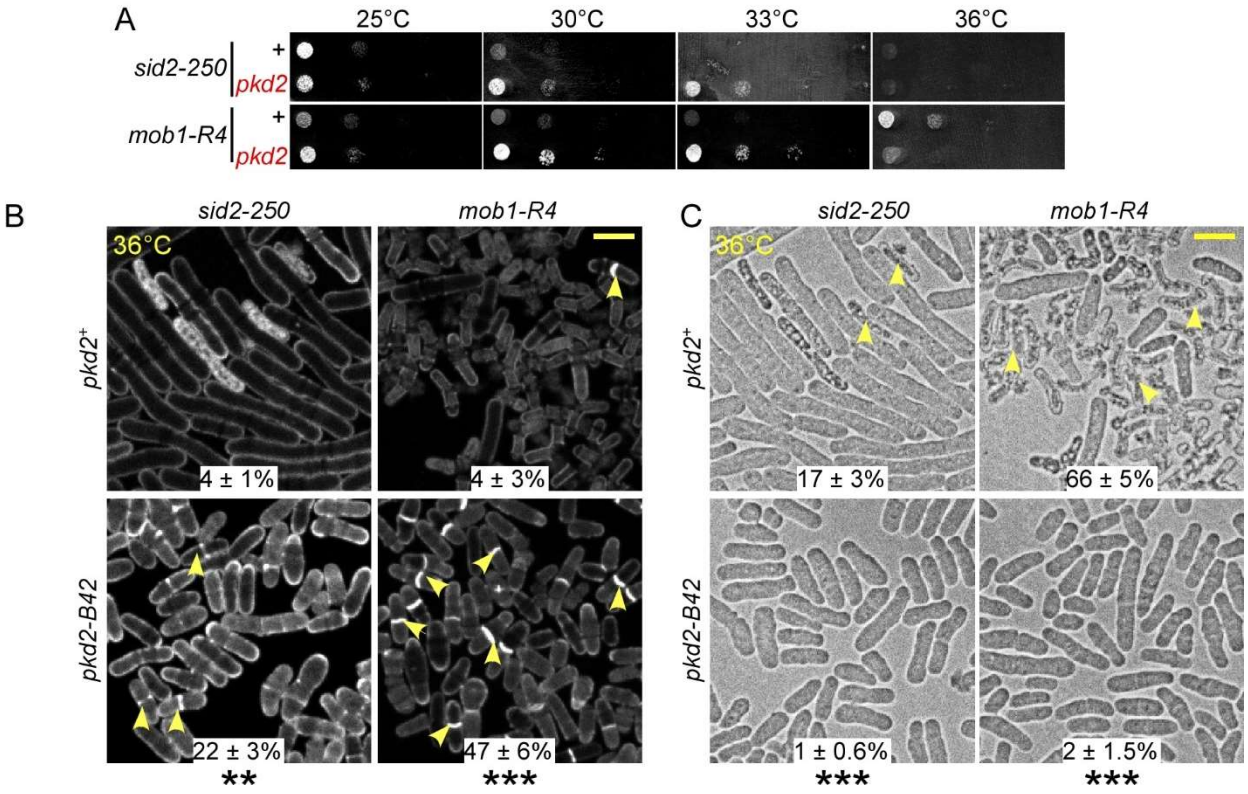


**Figure 5. SIN mutants are rescued by *pkd2-B42*.**

**(A)** Ten-fold dilution series of yeast cells at indicated temperatures.

**(B)** Fluorescence micrographs of either SIN (top) or *pkd2-B42* SIN (bottom) mutants fixed and stained with calcofluor to visualize septum.

**(C)** Bright-field micrographs of the SIN (top) and SIN *pkd2* mutant (bottom) cells at the restrictive temperature of 36°C. The numbers represent the percentage of septated or lysed cells (average ± standard deviations). Arrow heads point to the septated (B) or lysed (C) cells. The data was pooled from three independent biological repeats (n > 500). Scale bar represents length of 10µm. **:P<0.01, ***:P<0.001

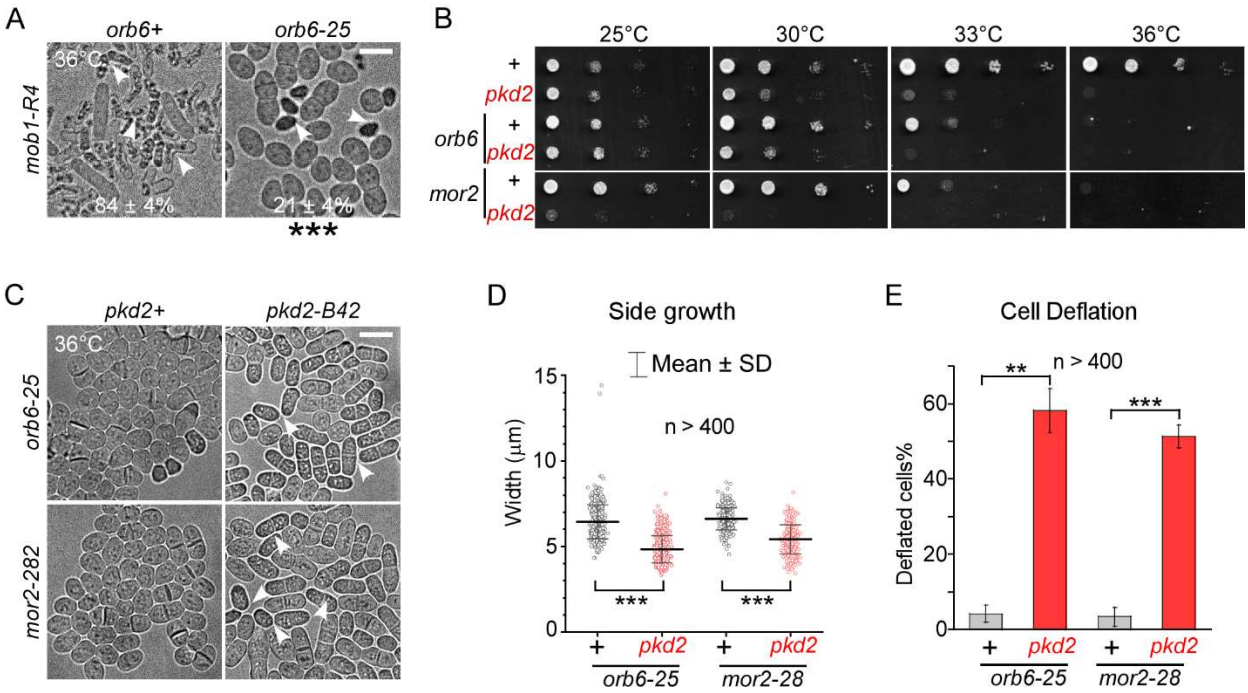


**Figure 6. Pkd2p synergizes with MOR pathway in promoting cell growth.**

**(A)** Micrograph of the mutants at the restrictive temperature (36°C). The numbers represent the percentage of lysed cells (average ± standard deviations).

**(B)** Ten-fold dilution series of yeast cells at indicated temperatures.

**(C-E)** *pkd2* mutation further inhibited the growth of *orb6* mutant cells. (C) Micrograph of the indicated mutants at 36°C. Arrowhead: deflated cells. (D) Dot plot showing the width of indicated mutant strains. (E) Bar graph showing fraction of the deflated cells. The data is pooled from two biological repeats (n > 400). Scale bar represents length of 10μm. **:P<0.01, ***:P<0.001

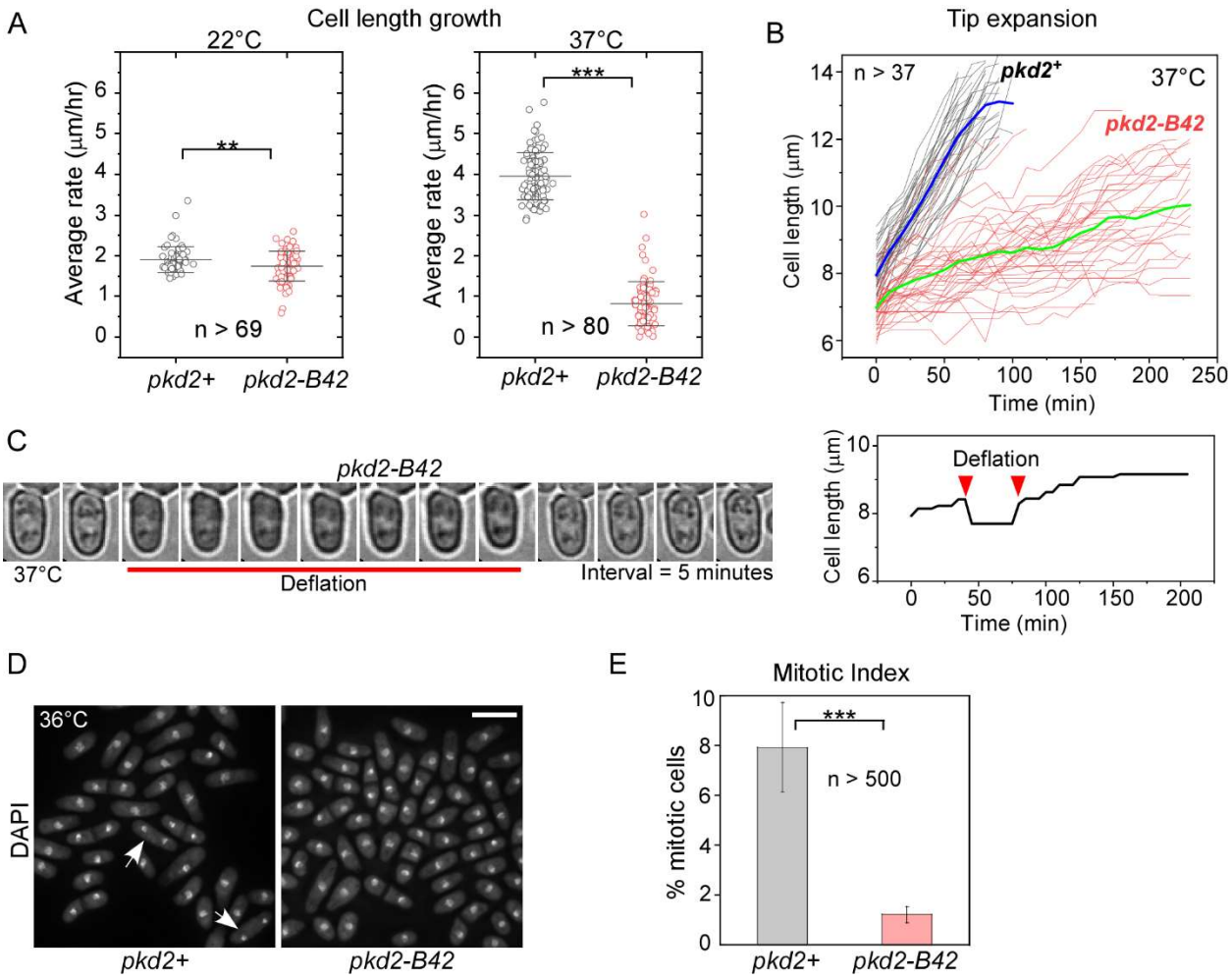


**Figure 7. Pkd2p is required for the cell size expansion during growth.**

**(A-B)** Tip expansion of *pkd2-B42* cells. (A) Dot plots of the average tip expansion rate among the wild-type and the *pkd2* mutant cells at either 22°C or 37°C. Lines represent average ± standard deviations. (B) Time courses of the tip expansion of individual wild-type (black lines) and *pkd2-B42* cells (red lines) at restrictive temperature. Blue (wild-type) and green (*pkd2-B42*) line represent the average time courses of tip expansion.

**(C)** Time-lapse micrograph of a *pkd2-B42* at 37°C. It underwent temporary deflation (red line) before resuming growth.

**(D)** Fluorescence micrographs of either wild-type (left) and *pkd2-B42* (right) cells fixed and stained with DAPI to visualize the nucleus.

**(E)** Bar Graphs of the mitotic index of *pkd2-B42* cells, compared to the wild-type. The data were pooled from at least two independent biological repeats. Scale bar represents length of 10µm **:P<0.01 ***: P < 0.001.

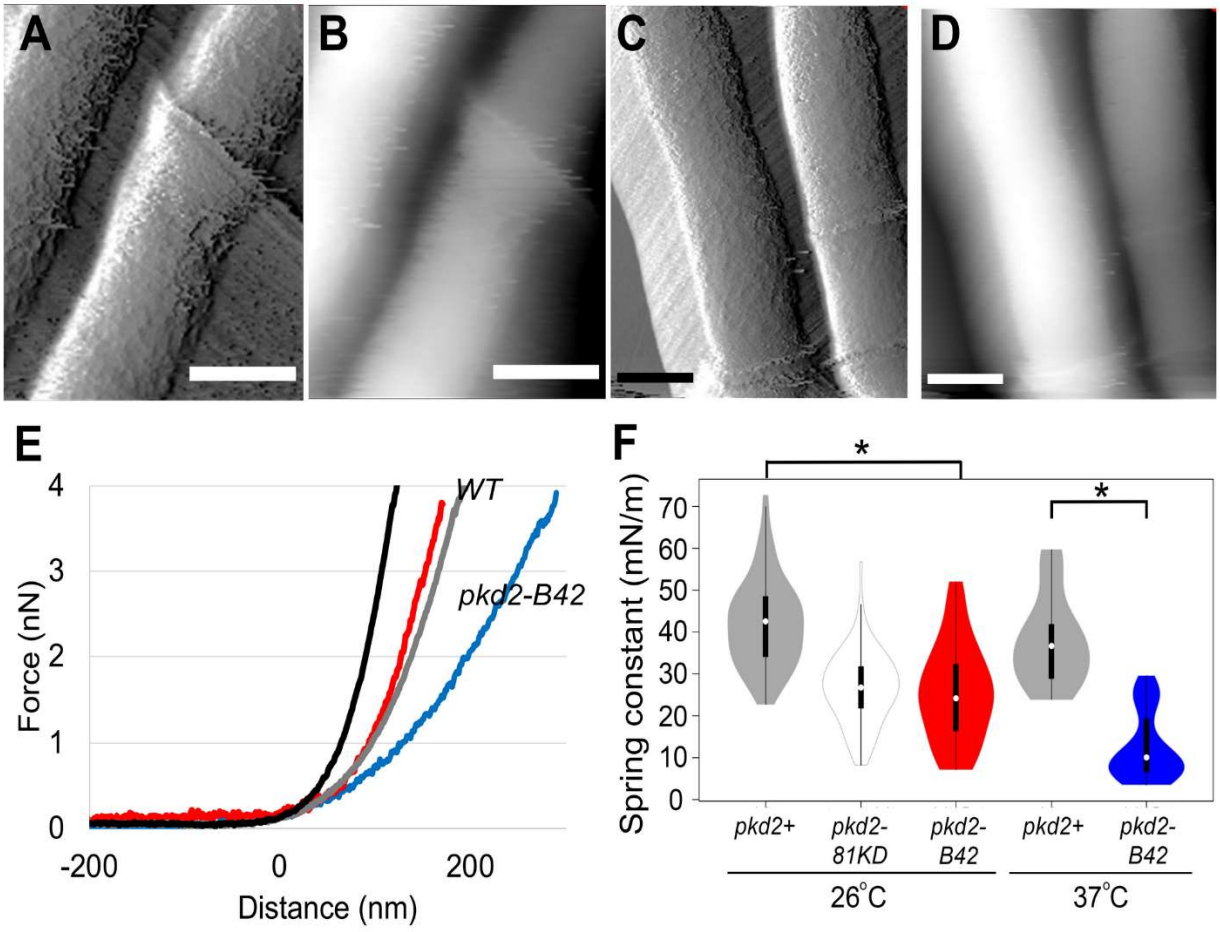


**Figure 8. Cellular stiffness is decreased in *pkd2* mutant cells.**

**(A-D)** Atomic Force Microscope (AFM) deflection (A, C) and height (B, D) images of wild-type (A, B) or *pkd2-B42* (C, D) cells acquired by intermittent contact imaging mode in EMM5S liquid media. Height scale (B, D) is 3µm; scale bar for all images is 2µm.

**(E)** Representative extension force curves from wild-type (black), *pkd2-81KD* (grey), or *pkd2-B42* (red) cell surface following incubation at 26°C, or *pkd2-B42* (blue) cell surface following incubation at 37°C. The horizontal linear region of each curve (-200 nm to 0 nm) reflects the cantilever approaching the surface with the zero point along the X-axis indicating the point of contact between the tip and surface. The linear deflection of the cantilever tip occurs as the cantilever tip pushes against the cell wall, which indicates the surface stiffness.

**(F)** Violin plot of cellular spring constants calculated from extension force curves at 26°C for wild-type (black), *pkd2-81KD* (grey), or *pkd2-B42* (red) cells, and at 37°C in wild-type (black) or *pkd2-B42* (blue) cells. The boxed region indicates the upper and lower quartiles for each data set; median is indicated by the horizontal line within the box; whiskers extend to the high and low data points. (n > 500, force measurements total from 5 cells per condition). Asterisks indicate $p < 1e^{-5}$, measured by ANOVA and student t-test).

## Supplemental materials:

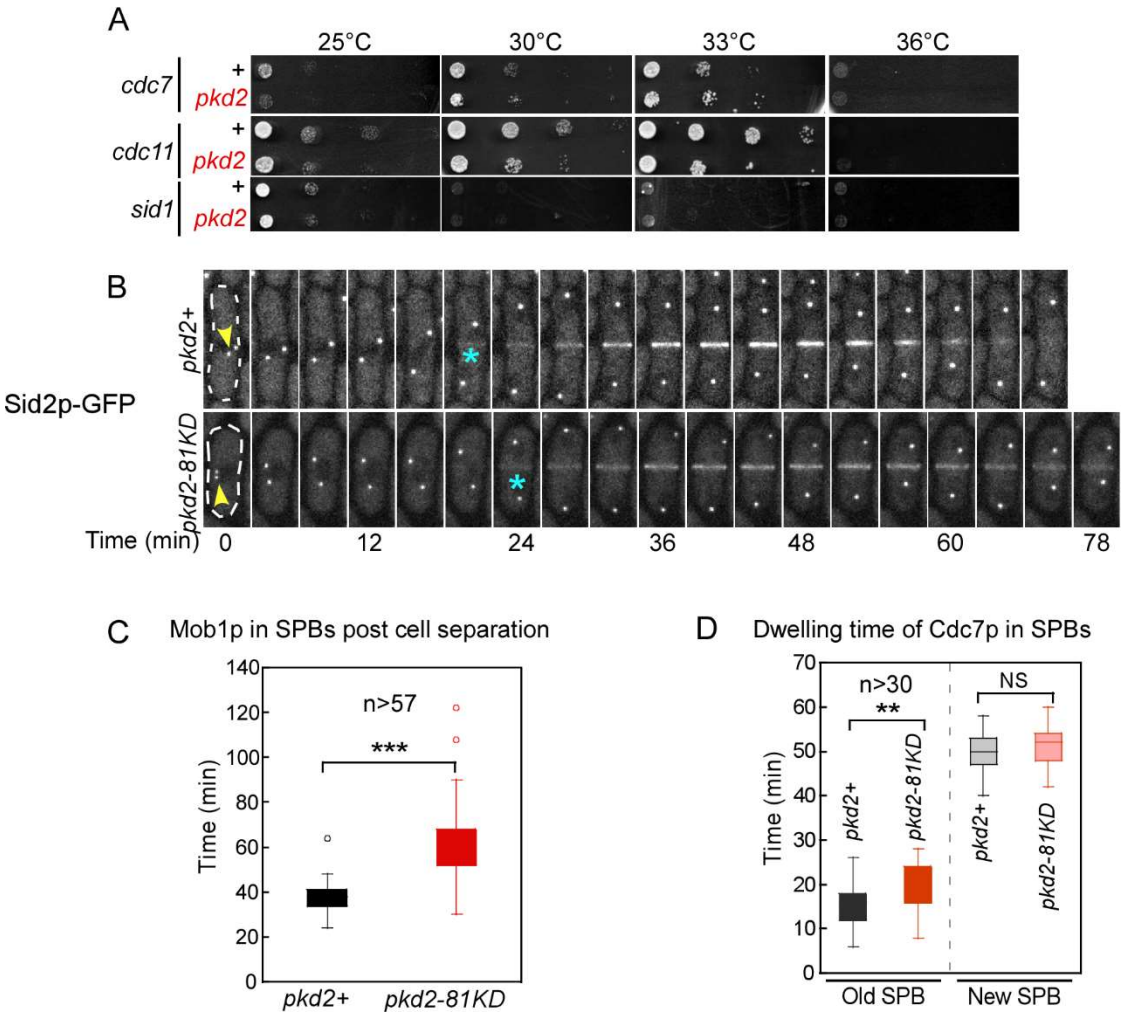


**Supplemental Figure S1. Genetic interaction between *pkd2* and SIN and localization of SIN proteins in *pkd2* mutant.**

**(A)** Ten-fold dilution series of yeast cells at indicated temperatures.

**(B)** Time-lapse micrographs of either a wild-type (top) or a *pkd2* mutant (bottom) cells expressing Mob1p-GFP. Number represents time in minutes after the SPB separation. Arrowhead: SPB separation, Asterisk*: Appearance at the division plane.

**(C)** Box plot showing the dwelling time of Mob1p-GFP after cell separation at the SPB of daughter cell pair in the wild-type and *pkd2* mutant cells (n>57).

**(D)** Box plot showing the dwelling time of Cdc7p-GFP at the SPBs in the wild-type and *pkd2*-mutant cells (n > 30). The data is pooled from two biological repeats. **: P<0.01, ***:P<0.001

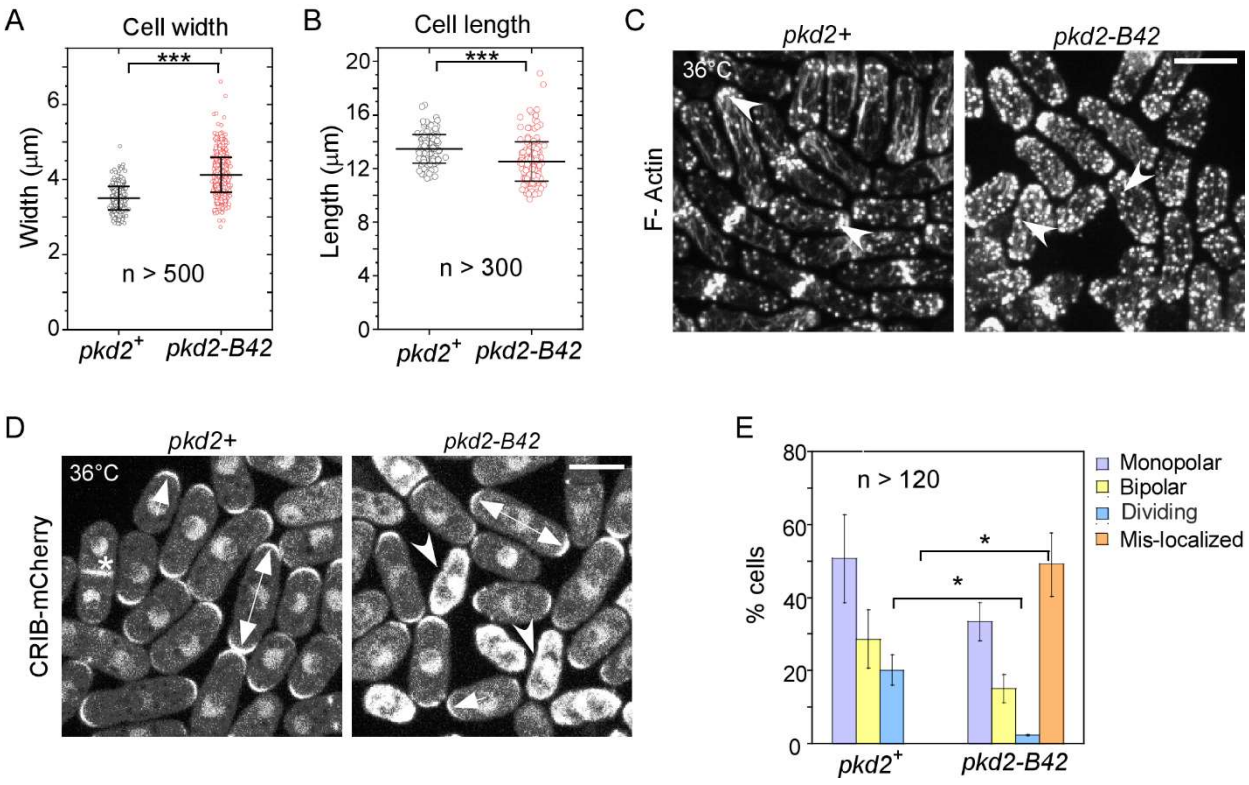


**Supplemental Figure S2. Morphological defects of *pkd2-B42* mutant.**

**(A-B)** Dot plots of the width (A) and length (B) of *pkd2-B42* cells, compared to the wild-type (*pkd2*$^{+}$).

**(C)** Fluorescent micrograph of bodipy-phallacidin stained wild-type and *pkd2-B42* cells to visualize actin filaments.

**(D)** Fluorescent micrograph of CRIB-mCherry in wild-type and *pkd2-B42* cell at 36°C. CRIB localization is classified as monopolar (arrow-single headed), bipolar (arrow-double headed), division plane (asterisk). *pkd2-B42* cells showed mis-localized CRIB (arrowhead) signal.

**(E)** Plot shows fraction of different polarity types in wild-type and *pkd2-B42* mutant cells. The data is pooled from two biological repeats. Scale bar represents length of 10µm. *: P<0.05, ***: P < 0.001

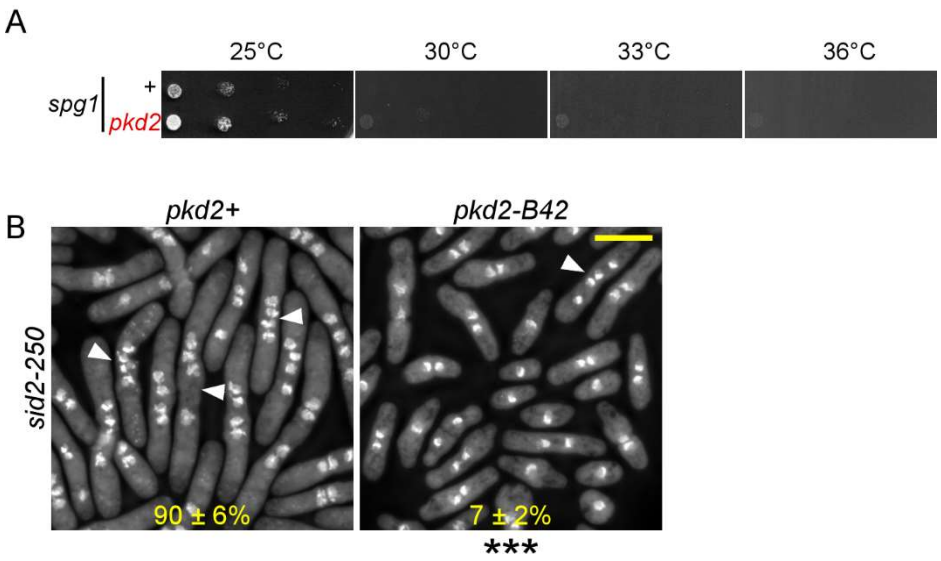


**Supplemental Figure S3. Genetic interaction between *pkd2-B42* and SIN mutants.**

**(A)** Ten-fold dilution series of yeast cells at indicated temperatures.

**(B)** Fluorescence micrographs of *sid2-250* (left) and *pkd2-B42 sid2-250* (right) cells fixed and stained with DAPI to visualize the nucleus. Numbers represent the percentage of multinucleated cells (average ± standard deviations). Arrow heads point to the multinucleated cells. The data was pooled from at least two independent biological repeats (n > 400). Scale bar represents length of 10μm. ***:P<0.001.

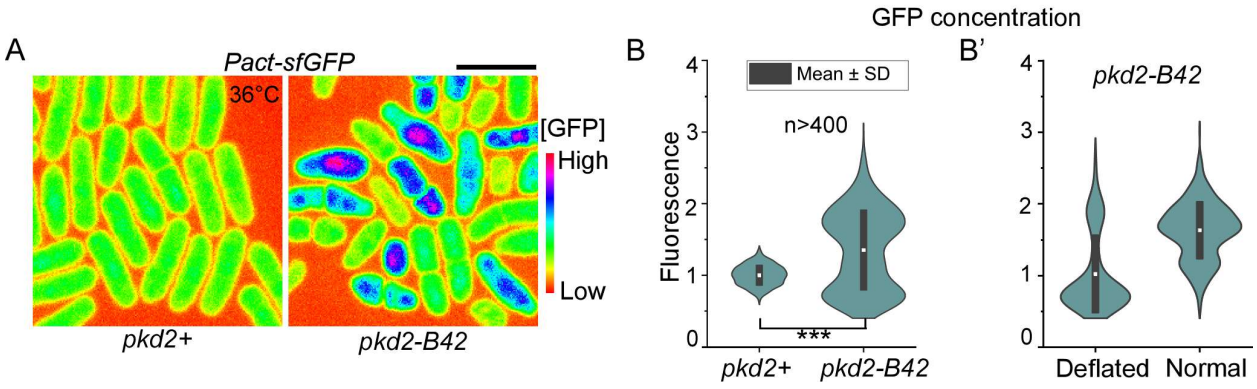


**Supplemental Figure S4. *pkd2-B42* has defect in volume expansion.**

**(A)** Fluorescence micrographs (spectrum-colored) of the wild-type (left) and *pkd2-B42* (right) cells at 36°C. Both constitutively expressed free diffusible sfGFP.

**(B)** Violin plots of intracellular GFP fluorescence. The lines represent average ± standard deviations. (B') Violin plots showing the intracellular GFP fluorescence in the deflated and normal looking *pkd2-B42* cells. The data were pooled from at two independent biological repeats. Scale bar represents length of 10μm. ***: $P < 0.001$.

619 **Supplemental movies:**

620 **Supplemental movie 1: Tip growth of wild-type cell at 37°C.** Time lapse of wild-type cell at
621 37°C showing tip expansion. Number represents time in minutes. $T_0$ = Cell Separation. Wild-
622 type cell expands at ~4µm/hour.

623 **Supplemental movie 2: Tip growth of *pkd2-B42* cell at 37°C.** Time lapse of *pkd2-B42* cell at
624 37°C showing tip expansion. Number represents time in minutes. $T_0$ = Cell Separation. *pkd2-B42*
625 cell expands at an average rate of 0.8µm/hour at this temperature.

626 **Supplemental movie 3: Deflation of pkd2-B42 cells at restrictive temperature.** Time lapse of
627 *pkd2-B42* cells at 37°C showing temporary cell shrinkage. Arrow points to the cell when it is in a
628 deflated state (undergoes cell shrinkage). Number represents time in minutes.

629

## References:


Arfsten, J., S. Leupold, C. Bradtmoller, I. Kampen, and A. Kwade. 2010. Atomic force microscopy studies on the nanomechanical properties of Saccharomyces cerevisiae. *Colloids Surf B Biointerfaces*. 79:284-290.

Arnoldi, M., M. Fritz, E. Bauerlein, M. Radmacher, E. Sackmann, and A. Boulbitch. 2000. Bacterial turgor pressure can be measured by atomic force microscopy. *Phys Rev E Stat Phys Plasmas Fluids Relat Interdiscip Topics*. 62:1034-1044.

Aydar, E., and C.P. Palmer. 2009. Polycystic kidney disease channel and synaptotagmin homologues play roles in schizosaccharomyces pombe cell wall synthesis/repair and membrane protein trafficking. *The Journal of membrane biology*. 229:141-152.

Balasubramanian, M.K., D. McCollum, L. Chang, K.C. Wong, N.I. Naqvi, X. He, S. Sazer, and K.L. Gould. 1998. Isolation and characterization of new fission yeast cytokinesis mutants. *Genetics*. 149:1265-1275.

Barr, M.M., and P.W. Sternberg. 1999. A polycystic kidney-disease gene homologue required for male mating behaviour in C. elegans. *Nature*. 401:386-389.

Beltraminelli, N., M. Murone, and V. Simanis. 1999. The S. pombe zfs1 gene is required to prevent septation if mitotic progression is inhibited. *Journal of cell science*. 112 Pt 18:3103-3114.

Bohnert, K.A., A.P. Grzegorzewska, A.H. Willet, C.W. Vander Kooi, D.R. Kovar, and K.L. Gould. 2013. SIN-dependent phosphoinhibition of formin multimerization controls fission yeast cytokinesis. *Genes & development*. 27:2164-2177.

Bok, J.W., T. Sone, L.B. Silverman-Gavrila, R.R. Lew, F.J. Bowring, D.E. Catcheside, and A.J. Griffiths. 2001. Structure and function analysis of the calcium-related gene spray in Neurospora crassa. *Fungal genetics and biology : FG & B*. 32:145-158.

Cai, J., X. Song, W. Wang, T. Watnick, Y. Pei, F. Qian, and D. Pan. 2018. A RhoA-YAP-c-Myc signaling axis promotes the development of polycystic kidney disease. *Genes & development*. 32:781-793.

Camargo, F.D., S. Gokhale, J.B. Johnnidis, D. Fu, G.W. Bell, R. Jaenisch, and T.R. Brummelkamp. 2007. YAP1 increases organ size and expands undifferentiated progenitor cells. *Curr Biol*. 17:2054-2060.

Chen, Q., and T.D. Pollard. 2011. Actin filament severing by cofilin is more important for assembly than constriction of the cytokinetic contractile ring. *The Journal of cell biology*. 195:485-498.

Cortes, J.C., M. Sato, J. Munoz, M.B. Moreno, J.A. Clemente-Ramos, M. Ramos, H. Okada, M. Osumi, A. Duran, and J.C. Ribas. 2012. Fission yeast Ags1 confers the essential septum strength needed for safe gradual cell abscission. *The Journal of cell biology*. 198:637-656.

Das, M., D.J. Wiley, X. Chen, K. Shah, and F. Verde. 2009. The conserved NDR kinase Orb6 controls polarized cell growth by spatial regulation of the small GTPase Cdc42. *Curr Biol*. 19:1314-1319.

Dey, S.K., and T.D. Pollard. 2018. Involvement of the septation initiation network in events during cytokinesis in fission yeast. *J Cell Sci*. 131.

Dong, J., G. Feldmann, J. Huang, S. Wu, N. Zhang, S.A. Comerford, M.F. Gayyed, R.A. Anders, A. Maitra, and D. Pan. 2007. Elucidation of a universal size-control mechanism in Drosophila and mammals. *Cell*. 130:1120-1133.

Fankhauser, C., J. Marks, A. Reymond, and V. Simanis. 1993. The S. pombe cdc16 gene is required both for maintenance of p34cdc2 kinase activity and regulation of septum formation: a link between mitosis and cytokinesis? *The EMBO journal*. 12:2697-2704.

Furge, K.A., K. Wong, J. Armstrong, M. Balasubramanian, and C.F. Albright. 1998. Byr4 and Cdc16 form a two-component GTPase-activating protein for the Spg1 GTPase that controls septation in fission yeast. *Curr Biol*. 8:947-954.

Garcia-Cortes, J.C., and D. McCollum. 2009. Proper timing of cytokinesis is regulated by Schizosaccharomyces pombe Etd1. *The Journal of cell biology*. 186:739-753.

Gibbs, E., J. Hsu, K. Barth, and J.W. Goss. 2021. Characterization of the nanomechanical properties of the fission yeast (Schizosaccharomyces pombe) cell surface by atomic force microscopy. *Yeast (Chichester, England)*.

Gonzalez-Perrett, S., K. Kim, C. Ibarra, A.E. Damiano, E. Zotta, M. Batelli, P.C. Harris, I.L. Reisin, M.A. Arnaout, and H.F. Cantiello. 2001. Polycystin-2, the protein mutated in autosomal dominant polycystic kidney disease (ADPKD), is a Ca2+-permeable nonselective cation channel. *Proceedings of the National Academy of Sciences of the United States of America*. 98:1182-1187.

Goss, J.W., S. Kim, H. Bledsoe, and T.D. Pollard. 2014. Characterization of the roles of Blt1p in fission yeast cytokinesis. *Molecular biology of the cell*. 25:1946-1957.

Goss, J.W., and C.B. Volle. 2020. Using Atomic Force Microscopy To Illuminate the Biophysical Properties of Microbes. *ACS Appl Bio Mater*. 3:143-155.

Goyal, A., and V. Simanis. 2012. Characterization of ypa1 and ypa2, the Schizosaccharomyces pombe orthologs of the peptidyl proyl isomerases that activate PP2A, reveals a role for Ypa2p in the regulation of cytokinesis. *Genetics*. 190:1235-1250.

Gupta, S., M. Govindaraghavan, and D. McCollum. 2014. Cross talk between NDR kinase pathways coordinates cytokinesis with cell separation in Schizosaccharomyces pombe. *Eukaryot Cell*. 13:1104-1112.

Gupta, S., S. Mana-Capelli, J.R. McLean, C.T. Chen, S. Ray, K.L. Gould, and D. McCollum. 2013. Identification of SIN pathway targets reveals mechanisms of crosstalk between NDR kinase pathways. *Curr Biol*. 23:333-338.

Hanaoka, K., F. Qian, A. Boletta, A.K. Bhunia, K. Piontek, L. Tsiokas, V.P. Sukhatme, W.B. Guggino, and G.G. Germino. 2000. Co-assembly of polycystin-1 and -2 produces unique cation-permeable currents. *Nature*. 408:990-994.

Hardy, E., and L. Tsiokas. 2020. Polycystins as components of large multiprotein complexes of polycystin interactors. *Cellular signalling*. 72:109640.

Hergovich, A. 2016. The Roles of NDR Protein Kinases in Hippo Signalling. *Genes (Basel)*. 7.

Huang, J., S. Wu, J. Barrera, K. Matthews, and D. Pan. 2005. The Hippo signaling pathway coordinately regulates cell proliferation and apoptosis by inactivating Yorkie, the Drosophila Homolog of YAP. *Cell*. 122:421-434.

Huang, K., D.R. Diener, A. Mitchell, G.J. Pazour, G.B. Witman, and J.L. Rosenbaum. 2007. Function and dynamics of PKD2 in Chlamydomonas reinhardtii flagella. *The Journal of cell biology*. 179:501-514.

Hughes, J., C.J. Ward, B. Peral, R. Aspinwall, K. Clark, J.L. San Millan, V. Gamble, and P.C. Harris. 1995. The polycystic kidney disease 1 (PKD1) gene encodes a novel protein with multiple cell recognition domains. *Nature genetics*. 10:151-160.

Jin, Q.W., and D. McCollum. 2003. Scw1p antagonizes the septation initiation network to regulate septum formation and cell separation in the fission yeast Schizosaccharomyces pombe. *Eukaryot Cell*. 2:510-520.

Jin, Q.W., S. Ray, S.H. Choi, and D. McCollum. 2007. The nucleolar Net1/Cfi1-related protein Dnt1 antagonizes the septation initiation network in fission yeast. *Molecular biology of the cell*. 18:2924-2934.

Jin, Q.W., M. Zhou, A. Bimbo, M.K. Balasubramanian, and D. McCollum. 2006. A role for the septation initiation network in septum assembly revealed by genetic analysis of sid2-250 suppressors. *Genetics*. 172:2101-2112.

Johnson, A.E., D. McCollum, and K.L. Gould. 2012. Polar opposites: Fine-tuning cytokinesis through SIN asymmetry. *Cytoskeleton (Hoboken)*. 69:686-699.

Karagiannis, J., R. Oulton, and P.G. Young. 2002. The Scw1 RNA-binding domain protein regulates septation and cell-wall structure in fission yeast. *Genetics*. 162:45-58.

Knapp, B.D., P. Odermatt, E.R. Rojas, W. Cheng, X. He, K.C. Huang, and F. Chang. 2019. Decoupling of Rates of Protein Synthesis from Cell Expansion Leads to Supergrowth. *Cell Syst*. 9:434-445 e436.

Lew, R.R. 2011. How does a hypha grow? The biophysics of pressurized growth in fungi. *Nat Rev Microbiol*. 9:509-518.

Li, Y., L. He, N.A.P. Gonzalez, J. Graham, C. Wolgemuth, D. Wirtz, and S.X. Sun. 2017. Going with the Flow: Water Flux and Cell Shape during Cytokinesis. *Biophysical journal*. 113:2487-2495.

Lima, W.C., A. Vinet, J. Pieters, and P. Cosson. 2014. Role of PKD2 in rheotaxis in Dictyostelium. *PLoS One*. 9:e88682.

Liu, P., X. Lou, J.L. Wingfield, J. Lin, D. Nicastro, and K. Lechtreck. 2020. Chlamydomonas PKD2 organizes mastigonemes, hair-like glycoprotein polymers on cilia. *The Journal of cell biology*. 219.

Liu, X., T. Vien, J. Duan, S.H. Sheu, P.G. DeCaen, and D.E. Clapham. 2018. Polycystin-2 is an essential ion channel subunit in the primary cilium of the renal collecting duct epithelium. *eLife*. 7.

Ma, Y., R. Sugiura, A. Koike, H. Ebina, S.O. Sio, and T. Kuno. 2011. Transient receptor potential (TRP) and Cch1-Yam8 channels play key roles in the regulation of cytoplasmic Ca2+ in fission yeast. *PLoS One*. 6:e22421.

Miettinen, T.P., J.H. Kang, L.F. Yang, and S.R. Manalis. 2019. Mammalian cell growth dynamics in mitosis. *eLife*. 8.

Minc, N., A. Boudaoud, and F. Chang. 2009. Mechanical forces of fission yeast growth. *Curr Biol*. 19:1096-1101.

Mochizuki, T., G. Wu, T. Hayashi, S.L. Xenophontos, B. Veldhuisen, J.J. Saris, D.M. Reynolds, Y. Cai, P.A. Gabow, A. Pierides, W.J. Kimberling, M.H. Breuning, C.C. Deltas, D.J. Peters, and S. Somlo. 1996. PKD2, a gene for polycystic kidney disease that encodes an integral membrane protein. *Science (New York, N.Y)*. 272:1339-1342.

Morris, Z., D. Sinha, A. Poddar, B. Morris, and Q. Chen. 2019. Fission yeast TRP channel Pkd2p localizes to the cleavage furrow and regulates cell separation during cytokinesis. *Molecular biology of the cell*. 30:1791-1804.

Moser, M.J., M.R. Flory, and T.N. Davis. 1997. Calmodulin localizes to the spindle pole body of Schizosaccharomyces pombe and performs an essential function in chromosome segregation. *Journal of cell science*. 110 ( Pt 15):1805-1812.

Munoz, J., J.C. Cortes, M. Sipiczki, M. Ramos, J.A. Clemente-Ramos, M.B. Moreno, I.M. Martins, P. Perez, and J.C. Ribas. 2013. Extracellular cell wall beta(1,3)glucan is required to couple septation to actomyosin ring contraction. *The Journal of cell biology*. 203:265-282.

Palmer, C.P., E. Aydar, and M.B. Djamgoz. 2005. A microbial TRP-like polycystic-kidney-disease-related ion channel gene. *The Biochemical journal*. 387:211-219.

Poddar, A., O. Sidibe, A. Ray, and Q. Chen. 2021. Calcium spikes accompany cleavage furrow ingression and cell separation during fission yeast cytokinesis. *Molecular biology of the cell*. 32:15-27.

Pollard, T.D., and J.Q. Wu. 2010. Understanding cytokinesis: lessons from fission yeast. *Nature reviews*. 11:149-155.

Protchenko, O., R. Rodriguez-Suarez, R. Androphy, H. Bussey, and C.C. Philpott. 2006. A screen for genes of heme uptake identifies the FLC family required for import of FAD into the endoplasmic reticulum. *The Journal of biological chemistry*. 281:21445-21457.

Ray, S., K. Kume, S. Gupta, W. Ge, M. Balasubramanian, D. Hirata, and D. McCollum. 2010. The mitosis-to-interphase transition is coordinated by cross talk between the SIN and MOR pathways in Schizosaccharomyces pombe. *The Journal of cell biology*. 190:793-805.

Rigamonti, M., S. Groppi, F. Belotti, R. Ambrosini, G. Filippi, E. Martegani, and R. Tisi. 2015. Hypotonic stress-induced calcium signaling in Saccharomyces cerevisiae involves TRP-like transporters on the endoplasmic reticulum membrane. *Cell calcium*. 57:57-68.

Salimova, E., M. Sohrmann, N. Fournier, and V. Simanis. 2000. The S. pombe orthologue of the S. cerevisiae mob1 gene is essential and functions in signalling the onset of septum formation. *Journal of cell science*. 113 ( Pt 10):1695-1704.

Schmidt, S., M. Sohrmann, K. Hofmann, A. Woollard, and V. Simanis. 1997. The Spg1p GTPase is an essential, dosage-dependent inducer of septum formation in Schizosaccharomyces pombe. *Genes & development*. 11:1519-1534.

Silverman-Gavrila, L.B., and R.R. Lew. 2003. Calcium gradient dependence of Neurospora crassa hyphal growth. *Microbiology (Reading)*. 149:2475-2485.

Simanis, V. 2015. Pombe's thirteen - control of fission yeast cell division by the septation initiation network. *Journal of cell science*. 128:1465-1474.

Sohrmann, M., S. Schmidt, I. Hagan, and V. Simanis. 1998. Asymmetric segregation on spindle poles of the Schizosaccharomyces pombe septum-inducing protein kinase Cdc7p. *Genes & development*. 12:84-94.

Sparks, C.A., M. Morphew, and D. McCollum. 1999. Sid2p, a spindle pole body kinase that regulates the onset of cytokinesis. *The Journal of cell biology*. 146:777-790.

Stephenson, K.S., N.A. Gow, F.A. Davidson, and G.M. Gadd. 2014. Regulation of vectorial supply of vesicles to the hyphal tip determines thigmotropism in Neurospora crassa. *Fungal Biol*. 118:287-294.

Su, Q., F. Hu, X. Ge, J. Lei, S. Yu, T. Wang, Q. Zhou, C. Mei, and Y. Shi. 2018. Structure of the human PKD1-PKD2 complex. *Science (New York, N.Y)*. 361.

Ta, C.M., T.N. Vien, L.C.T. Ng, and P.G. DeCaen. 2020. Structure and function of polycystin channels in primary cilia. *Cellular signalling*. 72:109626.

Tang, X., J. Huang, A. Padmanabhan, K. Bakka, Y. Bao, B.Y. Tan, W.Z. Cande, and M.K. Balasubramanian. 2011. Marker reconstitution mutagenesis: a simple and efficient reverse genetic approach. *Yeast (Chichester, England)*. 28:205-212.

Tatebe, H., K. Nakano, R. Maximo, and K. Shiozaki. 2008. Pom1 DYRK regulates localization of the Rga4 GAP to ensure bipolar activation of Cdc42 in fission yeast. *Curr Biol*. 18:322-330.

Tay, Y.D., M. Leda, C. Spanos, J. Rappsilber, A.B. Goryachev, and K.E. Sawin. 2019. Fission Yeast NDR/LATS Kinase Orb6 Regulates Exocytosis via Phosphorylation of the Exocyst Complex. *Cell reports*. 26:1654-1667 e1657.

Thevenaz, P., U.E. Ruttimann, and M. Unser. 1998. A pyramid approach to subpixel registration based on intensity. *IEEE Trans Image Process*. 7:27-41.

Verde, F., D.J. Wiley, and P. Nurse. 1998. Fission yeast orb6, a ser/thr protein kinase related to mammalian rho kinase and myotonic dystrophy kinase, is required for maintenance of cell polarity and coordinates cell morphogenesis with the cell cycle. *Proceedings of the National Academy of Sciences of the United States of America*. 95:7526-7531.

Volle, C.B., M.A. Ferguson, K.E. Aidala, E.M. Spain, and M.E. Nunez. 2008. Spring constants and adhesive properties of native bacterial biofilm cells measured by atomic force microscopy. *Colloids Surf B Biointerfaces*. 67:32-40.

Watnick, T.J., Y. Jin, E. Matunis, M.J. Kernan, and C. Montell. 2003. A flagellar polycystin-2 homolog required for male fertility in Drosophila. *Curr Biol*. 13:2179-2184.

Willet, A.H., A.K. DeWitt, J.R. Beckley, D.M. Clifford, and K.L. Gould. 2019. NDR Kinase Sid2 Drives Anillin-like Mid1 from the Membrane to Promote Cytokinesis and Medial Division Site Placement. *Curr Biol*. 29:1055-1063 e1052.

817 Wood, C.R., Z. Wang, D. Diener, J.M. Zones, J. Rosenbaum, and J.G. Umen. 2012. IFT proteins
818 accumulate during cell division and localize to the cleavage furrow in Chlamydomonas. *PLoS*
819 *One*. 7:e30729.
820 Wu, J.Q., J.R. Kuhn, D.R. Kovar, and T.D. Pollard. 2003. Spatial and temporal pathway for assembly and
821 constriction of the contractile ring in fission yeast cytokinesis. *Developmental cell*. 5:723-734.
822 Wu, J.Q., V. Sirotkin, D.R. Kovar, M. Lord, C.C. Beltzner, J.R. Kuhn, and T.D. Pollard. 2006. Assembly of
823 the cytokinetic contractile ring from a broad band of nodes in fission yeast. *The Journal of cell*
824 *biology*. 174:391-402.
825 Yoshida, T., T. Toda, and M. Yanagida. 1994. A calcineurin-like gene ppb1+ in fission yeast: mutant
826 defects in cytokinesis, cell polarity, mating and spindle pole body positioning. *Journal of cell*
827 *science*. 107 ( Pt 7):1725-1735.
828 Yu, F.X., B. Zhao, and K.L. Guan. 2015. Hippo Pathway in Organ Size Control, Tissue Homeostasis, and
829 Cancer. *Cell*. 163:811-828.

830